Drug Design, Development and Therapy

Dovepress
Taylor & Francis Group

Open Access Full Text Article

ORIGINAL RESEARCH

Biochemical and Molecular Studies on the Role of Celecoxib and Some Related Bipyrazoles in Mitigating Induced Liver Injury in Experimental Animals

Maram Marei[1], Nefertiti El-Nikhely[1], Eman Sheta[2], Hanan Ragab[3], Ahmed Wahid[4], Hesham Saeed[1], Sherif AF Rostom[3]

[1]Department of Biotechnology, Institute of Graduate Studies and Research, Alexandria University, Alexandria, 21521, Egypt; [2]Department of Pathology, Faculty of Medicine, Alexandria University, Alexandria, 21521, Egypt; [3]Department of Pharmaceutical Chemistry, Faculty of Pharmacy, Alexandria University, Alexandria, 21521, Egypt; [4]Department of Pharmaceutical Biochemistry, Faculty of Pharmacy, Alexandria University, Alexandria, 21521, Egypt

Correspondence: Sherif AF Rostom, Email sherif.rostom@alexu.edu.eg

Introduction: Liver fibrosis is a life-threatening disease that greatly impacts the morbidity and mortality of hepatic patients worldwide, resulting mainly as a consequence of hepatitis C, alcoholic and non-alcoholic fatty liver. COX-1 and COX-2 isozymes catalyze the synthesis of prostaglandins (PGs) and thromboxanes (TXs) from arachidonic acid causing inflammation. Owing to the scarcity of approved fibrolytic drugs available for human use, celecoxib (a selective COX-2 inhibitor) has been repurposed as a potential antifibrotic and fibrolytic agent in some chronic liver fibrosis models.

Methods: The present study aims to discover a non-invasive treatment for liver fibrosis through investigating the possible ability of three celecoxib-related bipyrazole compounds **HR1-3** to reverse chemically induced liver fibrosis in rats using CCl_4. This fibrolytic effect was verified by histopathological, immunohistochemical, biochemical and biomolecular assays. In addition, in silico computer-aided evaluation of the compounds' binding mode to certain molecular targets was performed, and the in silico physicochemical properties, drug likeness and pharmacokinetic parameters were predicted using web-based applications.

Results: The analogs **HR1-3** could serve as novel therapeutic candidates for the mitigation of liver fibrosis that deserves further derivatizations and investigations. In particular, the fluorinated analog **HR3** proved to be the most active member in this study when compared to celecoxib due to its distinguished histopathological and immunohistochemical investigation results, beside its antioxidant potential, as well as its reliable effects against some biomarkers, namely, MMP-9, TGF-β1, TIMP-1, IL-6 and TNF-α.

Conclusion: Based on the obtained results, the fluorinated analog **HR3** could serve as a novel therapeutic candidate for the amelioration of liver fibrosis that deserves further derivatizations and investigations.

Keywords: liver fibrosis, CCl_4, COX2, ELISA, RT-PCR, molecular modeling

Introduction

Fibrosis is a natural immune response distinguished by the overgrowth, hardening and/or scarring of various tissues due to excessive deposition of extracellular matrix components (ECM), such as collagen. Various stimuli including persisting infections, autoimmune reactions, allergic reactions, radiation, and tissue injury could induce chronic inflammatory reactions, which usually end with fibrosis.[1]

Fibrosis can occur at different sites and different organs, but lung and liver fibrosis are major health challenges. Liver fibrosis is a highly conserved and coordinated wound healing process that aims to maintain the integrity of the liver through simultaneous inflammation, remodeling and tissue repair. The causes of liver fibrosis are multifactorial including hepatitis C, non-alcoholic fatty liver, alcoholic liver and autoimmune diseases.[2] Advanced liver fibrosis can lead to the development of liver cirrhosis, and both are responsible for the high morbidity and mortality rates among chronic hepatic patients.[3]

Received: 13 December 2024
Accepted: 1 May 2025
Published: 15 May 2025

Graphical Abstract

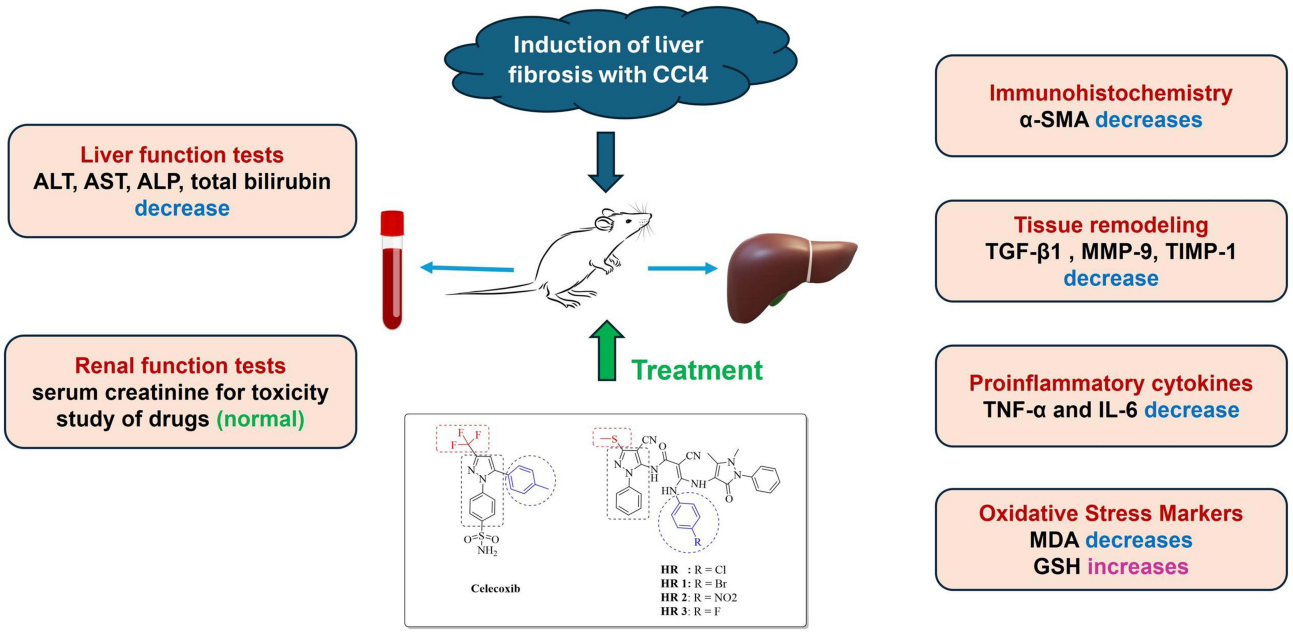

Currently, there is no effective anti-fibrotic treatment approved for human use, and liver transplantation still remains the only effective therapy.[4,5] However, liver fibrosis has been widely demonstrated to be reversible when the offending agent is removed.[5] Repetitive or long-lasting exposure to one or more of these injurious factors results in developing fibrogenesis by generating several profibrogenic mediators (eg cytokines, growth factors and others) that trigger the downstream effectors of fibrosis. Such effectors comprise activated hepatic stellate cells (aHSCs), myofibroblasts (MFBs) and Kupffer cells (KCs).[3]

Some studies have explained the association between inflammation and fibrosis. The inflammation of hepatocytes and the activation of the innate immune system lead to liver fibrosis caused by HSC activation. HSCs have been regarded as the main effector cells in liver fibrogenesis, as they receive a wide range of signals including transforming growth factor β1 (TGF-β1), which is the most fibrogenic agonist released from injured and/or dead hepatocytes and liver immune cells, predominantly the KCs.[6,7] Following their stimulation, the activated HSCs (aHSCs) migrate to the injured site, causing an upregulation of α-smooth muscle actin (α-SMA). Activated HSCs also release tissue inhibitors of metalloproteinases (TIMPs) 1 and 2 that inhibit the degrading action of matrix metalloproteinases (MMPs), thus promoting a deposition of ECM and producing a fibrous scar.[8–10]

During liver injury, the degradation of normal basement matrix and destruction of the connections between hepatocytes and basement usually occur due to the production of MMP-2 and MMP-9, which hinders the degradation of fibrillar collagens that accumulate in hepatic fibrosis.[11] Liver fibrosis has been linked to expressions of (MMP-2), where TGF-β induced HSCs proliferation in injured liver lead to up-regulation of MMP-2 expression and activity and can decrease the capacity for ECM remodeling.[12–14]

Furthermore, KCs initiate a fibrogenic response after repeated injury by recruiting additional innate immune cells to the site of injury. The infiltrating cells extensively secrete a broad spectrum of reactive oxygen species (ROS), cytokines and chemokines, which activate HSCs.[3,10,15] These cytokines and chemokines including tumor necrosis factor α (TNF-α) and interleukin 6 (IL-6) exert potent proinflammatory actions on HSCs. Meanwhile, others have direct profibrotic actions on HSCs and MFBs such as TGF-β1.[16]

Along the past decades, scientists alleged that liver fibrosis is an irreversible phenomenon. However, experimental and clinical studies proved that regression of liver fibrosis could occur when the offending agents including obesity, viruses (HBV & HCV), alcohol, and biliary obstruction are removed. The duration of this process depends on the cause and severity of liver fibrosis.[17] Notably, the reversal of advanced fibrosis or even cirrhosis could prevent the development of hepatic decompensation and diminishes the substantial risk of developing liver cancer. Nevertheless, reversal of liver fibrosis was not seen in around 15 to 25% of the patients who are effectively receiving antiviral medications. Furthermore, spontaneous reversal of liver fibrosis is usually too lengthy to prevent life-threatening problems.[3]

Cyclooxygenase (COX) is the rate limiting enzyme in inducing inflammation being responsible for the synthesis of prostaglandins (PGs) and thromboxanes (TXs) from arachidonic acid (AA).[18,19] There are two COX isozymes that have been acknowledged, namely, COX-1 and 2. COX-1 is omnipresent and constitutively expressed in several organs accounting for tissue homeostasis, whereas various tissues and cells exhibit low levels of COX-2, besides being inducible in response to different stimuli including inflammation, hormones, ROS, oncogenes, growth factors and hepatic diseases.[19–21] Long-term exposure to inflammatory stimuli, such as lipopolysaccharides (LPS) and TNF-α, induce the expression of COX-2 in hepatocytes.[18,19] Since the relationship between COX-2 expression and the progression of liver fibrosis was extensively studied, celecoxib (the most famous selective COX-2 inhibitor) has gained pronounced interest for its possible antifibrotic and fibrolytic effects on liver fibrosis and cirrhosis.[22,23] To date, several hypotheses were directed towards the deduction of the exact mechanism of fibrosis reversal through the selective inhibition of COX-2 by celecoxib.[11,24–27]

Chemically, celecoxib is a substituted pyrazole derivative, namely, 4-[5-(4-methylphenyl)–3-(trifluoromethyl)-1*H*-pyrazol-1-yl]benzenesulfonamide) (Figure 1).[28] Therefore, much attention has been focused on compounds comprising the pyrazole ring for their versatile and diverse biological activities.[29–32] Literature review revealed the ongoing efforts dedicated to the discovery of novel bioactive pyrazoles.[33–35] Especially, bipyrazoles endowed with anti-inflammatory potential carrying several functional groups and linked to various heterocyclic entities through different bridges.[36,37] Recently, a novel bipyrazole compound structurally related to celecoxib, namely; 3-(chlorophenylamino)-2-cyano-N-(4-cyano-3-(methylsulfanyl))-1-(phenyl-1*H*-pyrazol-5-yl)-3-(2,3-dihydro-1,5-dimethyl-3-oxo-2-phenyl-1*H*-pyrazol-4-ylamino)acrylamide (**HR**, Figure 1) has been proven to be a potential anti-inflammatory agent with a good affinity to COX-2 isozyme, beside its capability of inhibiting TNF-α and IL-1.[38,39] However, some restrictions on the clinical applicability of COX-2 inhibitors were developed owing to the reported cardiotoxicity and liability to thrombus formation side effects, probably due to their negative effect on the balance of the vasoactive eicosanoids such as prostacyclin and thromboxane.[40,41]

Inspired by the above-mentioned facts, the present study aims to discover a non-invasive treatment for liver fibrosis through investigating for the first time the possible ability of three celecoxib-related bipyrazoles with reported anti-inflammatory activities[42] to reverse chemically induced liver fibrosis. The targeted compounds (**HR1-3**, Figure 1) comprise the general pharmacophoric structural characteristics of selective COX-2 inhibitors that embrace a core carbocyclic or heterocyclic ring system surmounted with two vicinal aryl or hetaryl moieties with various substitutions.[43,44]

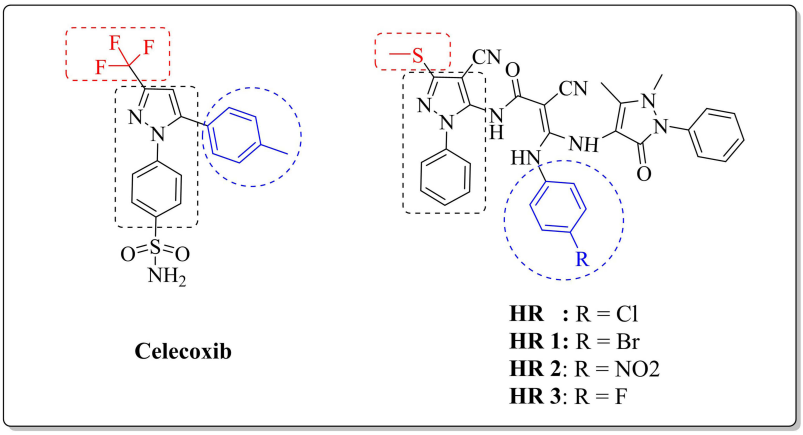

Figure 1 General structures of celecoxib and the three investigated bipyrazoles **HR1-3**.

https://doi.org/10.2147/DDDT.S512058

In this context, toxicity studies were conducted to assure the safety of the newly developed analogs, then their ability to mitigate liver fibrosis was verified by investigating their influence on TGF-β1 (the profibrogenic cytokine), IL-6 and TNF-α (the proinflammatory cytokines) and their effect on the MMP9 and TIMP-1 enzymes. Moreover, the impact of the three tested compounds on the histopathological changes including the deposition of α-SMA was also assessed. Furthermore, the biochemical assessment of hepatic biomarkers and the antioxidant profile of the tested compounds were also carried out. The obtained results were compared to the effects of celecoxib that is reported to possess an established fibrolytic potential. Finally, the binding mode and the possible molecular interactions of **HR1-3** with the active site of the TNF-α molecule were estimated via in silico molecular modelling. As a complementary process for lead optimization of the investigated compounds **HR1-3**, it was thought worthwhile to predict the in silico physicochemical properties, drug likeness and pharmacokinetic parameters using web-based applications.

Materials and Methods

Reagents and Chemicals

Carbon tetrachloride (CCl_4), 2-mercaptoethanol and thiobarbituric acid (TBA) were purchased from LOBA Chemie, Mumbai, India. Carboxymethylcellulose (CMC) was purchased from Adwic, Abu-Zaabal, Egypt. Formaldehyde was obtained from EL NASR Pharmaceutical Chemicals Co., Cairo, Egypt. Assay kits for Aspartate Aminotransferase (AST), Alanine Aminotransferase (ALT), Alkaline Phosphatase (ALP), Albumin, serum creatinine, total Bilirubin, cholesterol and triglycerides were purchased from Roche Diagnostics, Indianapolis, IN, USA. Enzyme-linked immunosorbent assay (ELISA) kit for tumor necrosis factor alpha (TNF-α) was obtained from Innova Biotech Co., Ltd., Beijing, China. 1,1,3,3-Tetramethoxypropane (Malonaldehyde bis(diethyl acetal)) and the ELISA kit for TIMP-1 (catalog number RAB0471) were purchased from Sigma Aldrich, St. Louis, Missouri, USA. Perchloric acid 70% ($HCLO_4$) was obtained from Central Drug House (CDH), New Delhi, India. Trichloroacetic acid (TCA) was purchased from SDFCL, Mumbai, India. Phosphate-Buffered Saline (PBS) was obtained from Lonza, Allendale, NJ, USA. Coomassie protein assay kit (catalog number 23200) was purchased from Thermo Scientific, Waltham, MA, USA. Assay kit of GSH was obtained from Biodiagnostic and Research Reagents, Giza, Egypt. QIAGEN RNeasy Mini kit was obtained from Qiagen, Germany; (catalog no. 74104, lot no. 157052104). Agarose was purchased from Piochem, Giza, Egypt. The reference standard celecoxib (Clx) was kindly gifted by Borg Pharmaceutical Industries, Alexandria, Egypt. The three investigated compounds (HR1-3) were synthesized according to previously reported procedures[42] in the Department of Pharmaceutical Chemistry, Faculty of Pharmacy, Alexandria University, Egypt.

Animals Experimental Design

Fifty-five healthy male Wistar rats of weights 130–160 g were kept in the animal house of the Institute of Graduate Studies and Research (IGSR), Alexandria University, Egypt. Rats were kept in a humidity-controlled room and under standard conditions of light (12 h light–dark cycles) and temperature, with free access to food and water. The animals were randomly divided into eleven groups (five rats each) for therapeutic and toxicity studies at the beginning of the experiment (Figures 2 and 3). The control group received a mixture of corn oil + carboxymethyl cellulose (CMC) in equivalent doses. Liver fibrosis was chemically induced by injecting 40% CCl_4 in corn oil intraperitoneally twice weekly for 6 weeks as reported by Chávez et al.[25] Rats were euthanized by decapitation under anesthesia by intraperitoneal injection (IP) of sodium thiopental (50 mg/kg).[45] This work was carried out under the **animal proposal AU14-200,922-1-8B**, approved by Alexandria University Institutional Animal Care and Use Committee (**Alexu-IACUC**). The "ICLAS (International Council for Laboratory Animal Science)" guidelines were followed for the welfare of the laboratory animals.[46]

Evaluation of Hepatic and Renal Biomarkers

Blood was collected through cardiac puncture into serum vacutainers, mixed well and centrifuged at 4000 rpm (Hettich Zentrifugen D 78532 Tuttlingen, Germany) for 10 minutes. The serum obtained was tested for the hepatic biomarkers: AST, ALT, ALP, albumin and total bilirubin were determined to detect changes in the liver function. The diagnostic kits were purchased from Roche Diagnostics, USA (Cat #: 20,764,949–322, 20,764,957–322, 03333752–190, 03183688–122

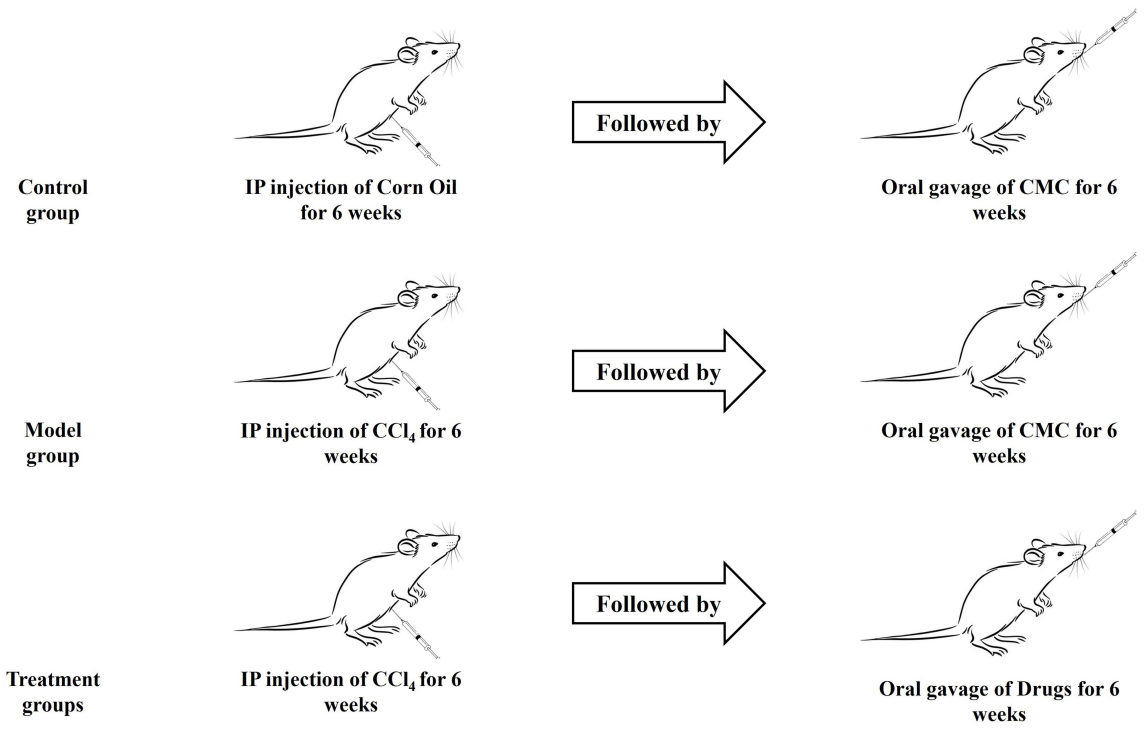

Figure 2 Animals experimental design.

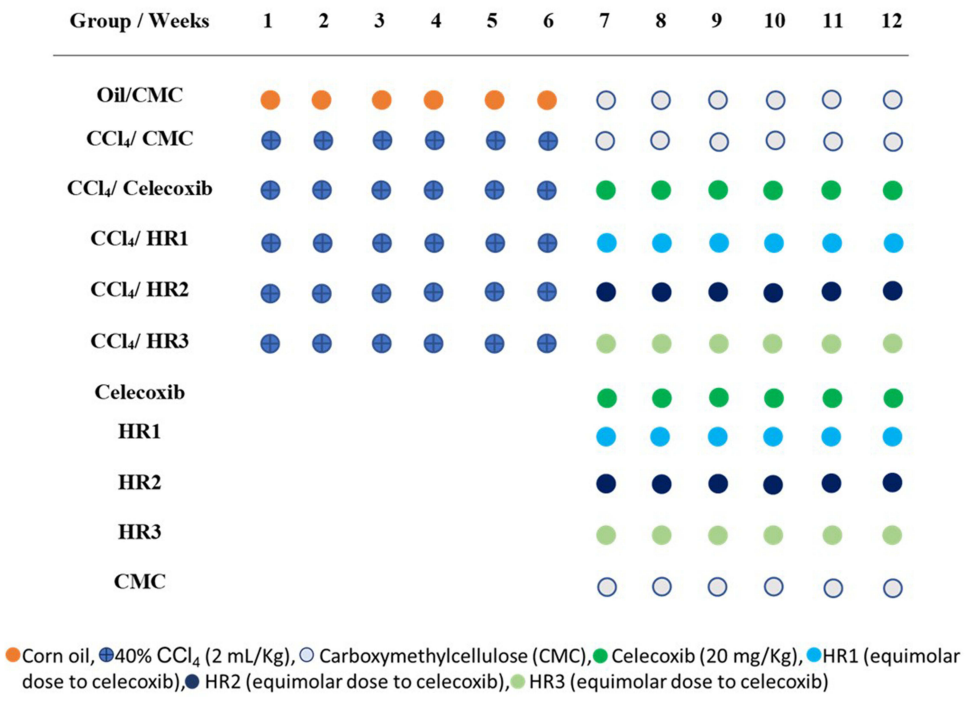

Figure 3 Dosage schedule given to different groups of experimental rats.

and 05795397–190, respectively). Meanwhile, serum creatinine levels were determined to assess kidney function using the kit of Cat # 04810716–190. All these tests were carried out according to the manufacturer's protocol, using a Roche/ Hitachi analyzer (cobas c 311, cobas c 501/502).

https://doi.org/10.2147/DDDT.S512058

Preparation of Rat Liver Tissues

Rat livers were harvested by dissection and washed with cold normal saline. Thereafter, a part of the liver was stored in 10% formaldehyde, then embedded in parafin to be sectioned into 4–5 μm sections for histological and immunohistochemical examinations. Another part of the liver was preserved in RNAlater solution (Qiagen, Germany, Mat. No. 1018087, lot no. 148052467) and stored at −20°C for Real-Time Quantitative Reverse Transcription Polymerase Chain Reaction (qRT-PCR). Finally, the remaining liver tissues were snap frozen using liquid nitrogen to be stored at −80°C for later biochemical and molecular analyses.

Histological and Immunohistochemical Tests

The sliced sections from the paraffin embedded formalin-fixed liver tissues were stained with Hematoxylin and Eosin for visualization of hepatocyte histology and inflammatory infiltrates. Meanwhile, to assess hepatic architecture and fibrosis, Masson's trichrome staining was employed, where each sample was independently assessed and scored by a pathologist blinded to the study. The scores of liver fibrosis degree were evaluated following the reported criteria[47] as follows: score zero denoted the absence of fibrosis, whereas score 1 indicated the presence of fibrous septea radiating from portal tracts or central veins. Meanwhile, score 2 designated the existence of collagen septea bridging between portal tracts and central veins, without noticeable nodules, whereas score 3 means focal nodular formation. Finally, nodular architecture and severe fibrosis were scored 4.

For immunohistochemical testing, sections (4 μm each) were cut and mounted on positively charged slides. They were stained by α-SMA monoclonal primary antibody (clone 1A4, ready to use, DAKO Co. Ltd. #IR611) using Dako auto Stainer (autostainer Link 48). Positive control (leiomyoma) was used in each run, whereas negative control was used by omitting the step of primary antibody. Assessment of immune-stained slides was performed, where ten high power fields of each section were photographed using a microscope-adopted camera. Thereafter, photos were analyzed using Image J software to record the immunopositive area (seen as brown staining) in each photo. The percentage of positive-stained area was calculated as the mean of the 10 examined photos for each rat liver sample.[48]

Biochemical Determination of Oxidative Stress Biomarkers in Liver Homogenates

Reduced Glutathione (GSH) Measurement

Liver GSH content was estimated using a colorimetric kit (Biodiagnostics, Egypt; Cat # GR 25 11) according to a reported method.[49] The developed yellow color was read against blank at λ_{max} 405 nm. Reduced glutathione levels were calculated according to the kit's provided formula as GSH (mg)/tissue (g):

$$\textbf{GSH concentration} = \frac{\text{Absorbance of the sample x } 66.66}{\text{Tissue weight in grams}}$$

Determination of Lipid Peroxides Levels

Lipid peroxides expressed as malondialdehyde (MDA) were estimated by the thiobarbituric acid method as previously reported.[50] Briefly, 0.5 mL of 40% tissue homogenate prepared in PBS was mixed with 1 mL of 0.8% TBA and 3 mL of 20% TCA. The mixture was heated in a boiling water bath for 20 minutes, left to cool then centrifuged at 3000 rpm for 10 minutes. The developed orange color was read against blank at λ_{max} 532 nm and calculated as nmol of MDA per gram tissue using a standard curve, where 1,1,3,3-tetramethoxypropane (serial dilution of 6 to 72 nM) was used as a standard for MDA.

Bradford Protein Determination

Bradford protein assay was carried out using Ready-To-Use Coomassie Blue G-250 Protein Assay Kit following the manufacturer's protocol to determine the protein content of each liver section used in this study. Standard Bovine Serum Albumin (BSA) stock solution of concentration 2 mg/mL was used to prepare a working solution of 50 μg/mL, followed by a 1:1 serial dilution using PBS (pH 7.4). In a 96 wells microplate, a 5 μL of the blank was pipetted into the first 2 wells, the following wells were filled with different concentrations of the standard BSA, followed by the tissue homogenate samples. Technical replicas were performed, then 250 μL of Coomassie reagent was added, mixed, and incubated for 10 minutes at room temperature. The absorbance of the blue color developed was measured using a microplate reader at λ_{max} 595 nm.

Enzyme-Linked Immunosorbent Assays (ELISA)

Innova Biotech, China; Cat # In-Ra1344, lot no. 202101, 202201 and Sigma Aldrich, MilliporeSigma, Burlington, MA, USA; Cat # RAB0471, lot no. 0930I708, 0914I708 ELISA kits were utilized to determine the concentrations TNF and TIMP-1, respectively, according to the manufacturer's protocol.

Real-Time PCR (RT-PCR)

The tissues kept in RNAlater solution were used for total RNA isolation using QIAGEN RNeasy Mini kit (Qiagen, Germany; catalog no. 74104, lot no. 157052104) according to manufacturer's protocol. The tissues were disrupted and homogenized using Qiagen tissue lyser LT for approximately 5 minutes. To get rid of genomic DNA, 80 µL of DNAse I (10 units of DNAse I in reconstitution buffer, pure gene DNAse I kit, Genetix Biotech, Asia; catalog no. PGM052, lot no. 362555), were added to each column for DNA digestion, and incubated at room temperature for 15 minutes. A standard agarose gel electrophoresis was carried out as conducted by Lee et al (2012) to confirm the integrity of the eluted RNA samples. RNA samples were run on 1% (w/v) agarose gel with ethidium bromide (0.1 µg/mL EtBr), the bands were visualized using a UV transilluminator.[51] The purified RNA samples were checked for purity, and concentration were determined by the ratio absorbance at λ_{max} 260 and 280 nm using NanoDrop™ 2000 spectrophotometer (Thermo Scientific). Thereafter, High-Capacity cDNA Reverse Transcription Kit was used according to the protocol to reverse transcribe 2 µg of pure RNA. The cDNA was then used to determine the expression levels of selected genes with RT-PCR. Such genes were detected using SYBR® Green PCR Master Mix kit (Applied Biosystems, Foster City, CA, USA). The primer sequences used in this study are listed in Table 1. The gene expression results were then analyzed using the $2^{-\Delta\Delta CT}$ method. Data were expressed as the mean fold changes ± SEM.

Molecular Modelling Studies

Molecular docking studies of the investigated compounds **HR1-3** were carried out using Molecular Operating Environment (MOE 2016.0802) software, Chemical Computing Group, Montreal, Canada (https://www.chemcomp.com/).

The X-ray crystal structures of TNF-α (PDB: 2AZ5) were downloaded from RCSB Protein Data Bank website.[52] The tested compounds were prepared by hydrogens addition, partial charges calculation and energy minimization through MMFF94x Force Field. In addition, preparation of the enzyme was performed by omitting the repeating chains, water molecules and any surfactants. For 3D protonation and calculation of partial charges and optimizing structural issues, MOE QuickPrep functionality was used. The default procedures in the MOE Dock protocol were used to detect the best binding poses and score values utilizing triangle matcher as a placement method and London dG as the main scoring function. An extra refinement step was also used by utilizing the rigid receptor method with affinity dG scoring function to obtain poses with the highest hydrophobic, and hydrogen-bond interactions with the enzyme. Moreover, the docking poses obtained in kcal/mol were evaluated, and interactions with the active site were examined. Finally, the best poses fitting into the binding site with the top scores and exhibiting good interactions with the enzyme were selected.[53]

Table 1 Sequences of Primers Used for Real-Time Quantitative PCR

Gene Symbol	Forward Primer Sequence	Reverse Primer Sequence
GAPDH	5`- GTA TTG GGC GCC TGG TCA CC –3`	5`- CGC TCC TGG AAG ATG GTG ATG G –3`
IL-6	5`- TGA TGG ATG CTT CCA AAC TG –3`	5`- GAG CAT TGG AAG TTG GGG TA –3`
MMP-9	5`- CAATCCTTGCAATGTGGATG –3`	5`- TAAGGAAGGGGCCCTGTAAT –3`
TGF-β1	5`- ATC CCT GCG ACC CAC ACA AG –3`	5`- CAA CTG CTT TGG AAG GAC TCG –3`

Abbreviations: GAPDH, glyceraldehyde 3-phosphate dehydrogenase; IL-6, interleukin 6; MMP-9, matrix metallopeptidase 9; TGF-β1, transforming growth factor beta1.

In silico Prediction of Physicochemical Properties, Drug-Likeness, Pharmacokinetics, and Toxicity Profile of Celecoxib Derivatives HR1-3

Prediction of the in silico physicochemical properties, drug likeness, pharmacokinetic parameters and toxicity profile of the investigated compounds **HR1-3** were carried out using the web-based applications Molinspiration (https://www.molinspiration.com/), and Osiris property explorer (https://www.organic-chemistry.org/prog/peo/) software. The ADME properties were also predicted using Pre-ADMET calculator software (https://preadmet.bmdrc.kr/).

Statistical Analysis

Statistical analyses were performed with GraphPad Prism 9 Software (GraphPad Prism Software, Inc). One way ANOVA with Tukey's multiple comparisons posttest was carried out for the assessment statistical significance of data. Outliers were identified using ROUT with Q = 1%. Data are expressed as mean ± SEM; statistical significance was set at p-value ≤ 0.05. Significance was noted as follows: * (P ≤ 0.05), ** (P ≤ 0.01), *** (P ≤ 0.001) and **** (P ≤ 0.0001).

Results

Bipyrazoles HR1-3 had No Hepato- or Renal Toxicity

The in vivo toxic effects of the drugs under investigation **HR1-3** were determined to ensure the safety of the selected doses. Close inspection of treated rats regarding signs of distress and agitation after receiving CMC, celecoxib and **HR1-3** was carried out daily. Their body weights were also recorded periodically (twice weekly) during the 6 weeks of the experiment. The rats did not show any signs of stress, toxicity or weight loss when receiving CMC, celecoxib and the tested compounds. On the contrary, the rats gained healthy weight throughout the experiment (Figure 4A).

Moreover, biochemical testing of liver biomarkers AST, ALT, ALP, total bilirubin and albumin showed normal levels indicating that the assigned doses would not cause harmful effect on the liver. Additionally, normal serum creatinine levels indicate the used doses to be kidney-safe (Table 2).

Gross examination of the rat livers of the toxicity groups receiving CMC, celecoxib, **HR1, HR2** and **HR3** showed normal smooth livers with no inflammation or fatty depositions and livers possessed normal liver consistency (Figure 4B). Liver tissues of treated rats displayed distinctively normal lobular architecture, with the hepatocytes radiating from the central veins. Masson's trichrome has stained the portal tracts, which appeared small and with sparse fibrous tissue around. These findings designated zero liver fibrosis score, indicating the lack of fibrogenic effect of the investigated drugs and/or the vehicle in question. Furthermore, the liver tissues displayed minimal α-SMA % that is normally deposited in liver as depicted in Figure 5.

HR1-3 Improved the Liver Function Tests in CCl_4 Induced Liver Fibrosis

To induce liver fibrosis, rats were injected intraperitoneally with 40% CCl_4 twice a week for 6 weeks followed by 6-week treatment by celecoxib or bipyrazoles **HR1-3** (20 mg/kg/day). Blood samples and livers were collected to assess the hepatic function, tissue remodeling and molecular changes.

Aminotransferases

It has been reported that the normal ranges of serum AST and ALT in rats are 50–150 U/L and 10–40 U/L, respectively.[54] In the present study, the model group showed elevated AST and ALT levels exceeding the normal ranges, indicating the presence of liver injury. Contrariwise, both AST and ALT levels of the control group fell within the reported normal range. Moreover, all the treatments by celecoxib or the tested compounds **HR1-3** caused a significant reduction in liver enzyme levels as shown in Figures 6A and 6B, confirming the reversal of liver injury.

Alkaline Phosphatase (ALP)

The reported normal range of serum ALP is from 30 to 130 U/L.[54] The obtained results indicated that liver fibrosis model group displayed a significant increase in ALP levels as it would affect liver parenchyma. Meanwhile, the ALP levels in the negative control group as well as the treatment groups (celecoxib and **HR1-3**) lied within the normal range (Figure 6C).

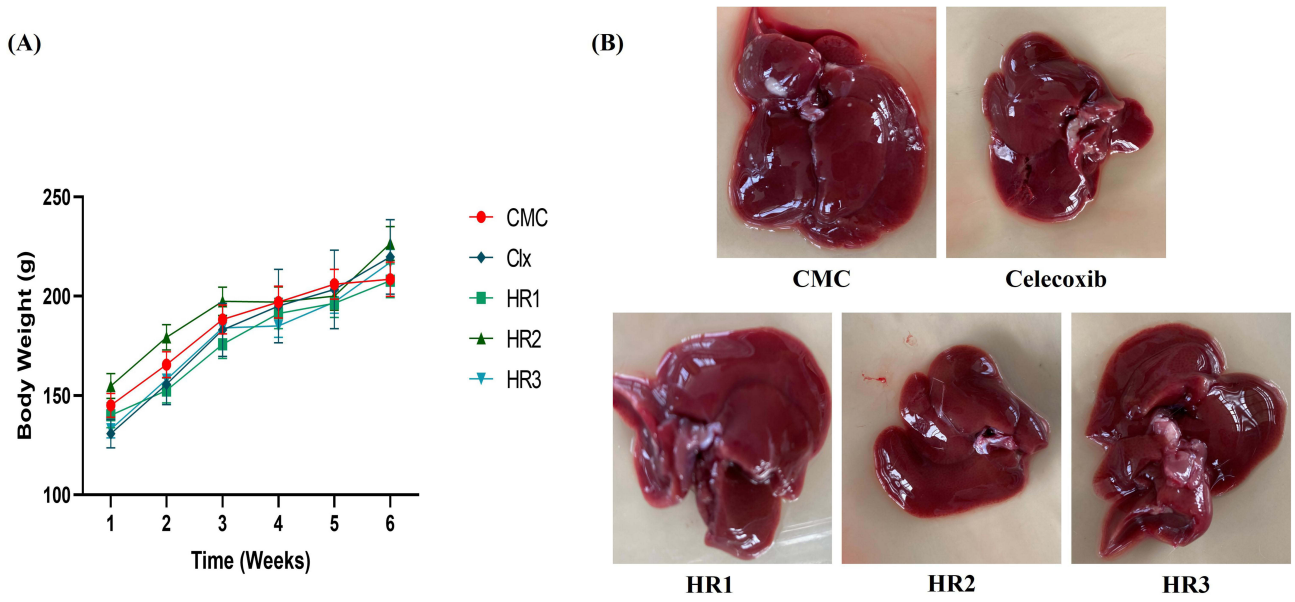

Figure 4 In vivo toxicity study. **(A)** Male Wistar rats' body weight along the six weeks of the experiment. Data are represented as mean ± SEM. No significant difference was noticed among the groups; n = 5. **(B)** Gross Examination of rat livers of in vivo toxicity groups.

Total Bilirubin (TBIL)

Total serum bilirubin is normally around 3.13 ± 0.13 µmol/L in the model group, which is equivalent to 0.035 ± 0.0015 mg/dL.[55] The obtained data revealed a significant elevation in the levels of total bilirubin in the model group pointing to the presence of liver damage, whereas the control group levels lied within the reported normal levels. The groups receiving celecoxib and the tested compounds **HR1-3** exhibited a significant decrease in the total serum bilirubin levels. Interestingly, compound **HR2** was almost equiactive with celecoxib in lowering TBIL serum levels, and superior to that of the analogs **HR1** and **HR3** (Figure 6D).

Fibrolytic Effects of the Bipyrazoles HR1-3 on the Induced Liver Fibrosis

Liver sections of control group (oil + CMC) stained with Hematoxylin and Eosin (H&E) showed normal lobular architecture, where the hepatocytes were radiating from the central veins. In contrast, the fibrosis model group that received CCl_4 + CMC showed total loss of architecture, as the hepatic parenchyma displayed multiple nodules of variable sizes separated by thick fibrous septea. These nodules are composed of proliferating hepatocytes arranged as cords without central veins. They also showed evident degenerative changes in the form of Councilman bodies, feathery cytoplasm, and foci of lobular inflammation. On the other hand, celecoxib (the standard reference drug) and the tested compounds **HR1-3** demonstrated evident fibrolytic effects in rats treated with CCl_4. The examined liver biopsies exhibited partial to total restoration of normal architecture, where the hepatocytes were seen arranged as cords radiating from the central veins. Additionally, the degenerative changes and the detected inflammation were notably diminished to the least possible.

Table 2 Hepatic and Renal Biomarkers of the in vivo Toxicity Study Groups

	Vehicle Control (CMC)	CLX	HR1	HR2	HR3
AST (U/L)	150.4 ± 9.53	127.5 ± 14	148.33 ± 4.66	123.33 ± 10.2	142 ± 7.37
ALT (U/L)	32.33 ± 2.73	45.66 ± 0.88	37.33 ± 5.81	35 ± 3	37.66 ± 2.33
ALP (U/L)	125.25 ± 6.56	123 ± 6.59	120.25 ± 18.9	121 ± 11.14	102.2 ± 6.36
Total Bilirubin (mg/dL)	0.05 ± 0.003	0.045 ± 0.006	0.07 ± 0.005	0.065 ± 0.009	0.037 ± 0.004
Albumin (g/dL)	3.72 ± 0.09	3.68 ± 0.04	3.35 ± 0.17	3.61 ± 0.23	3.7 ± 0.08
Creatinine (mg/dL)	0.44 ± 0.056	0.43 ± 0.06	0.39 ± 0.04	0.59 ± 0.06	0.53 ± 0.07

Notes: Values are expressed as a mean ± SEM; (n = 5), No significant difference was recognized between the groups.

https://doi.org/10.2147/DDDT.S512058

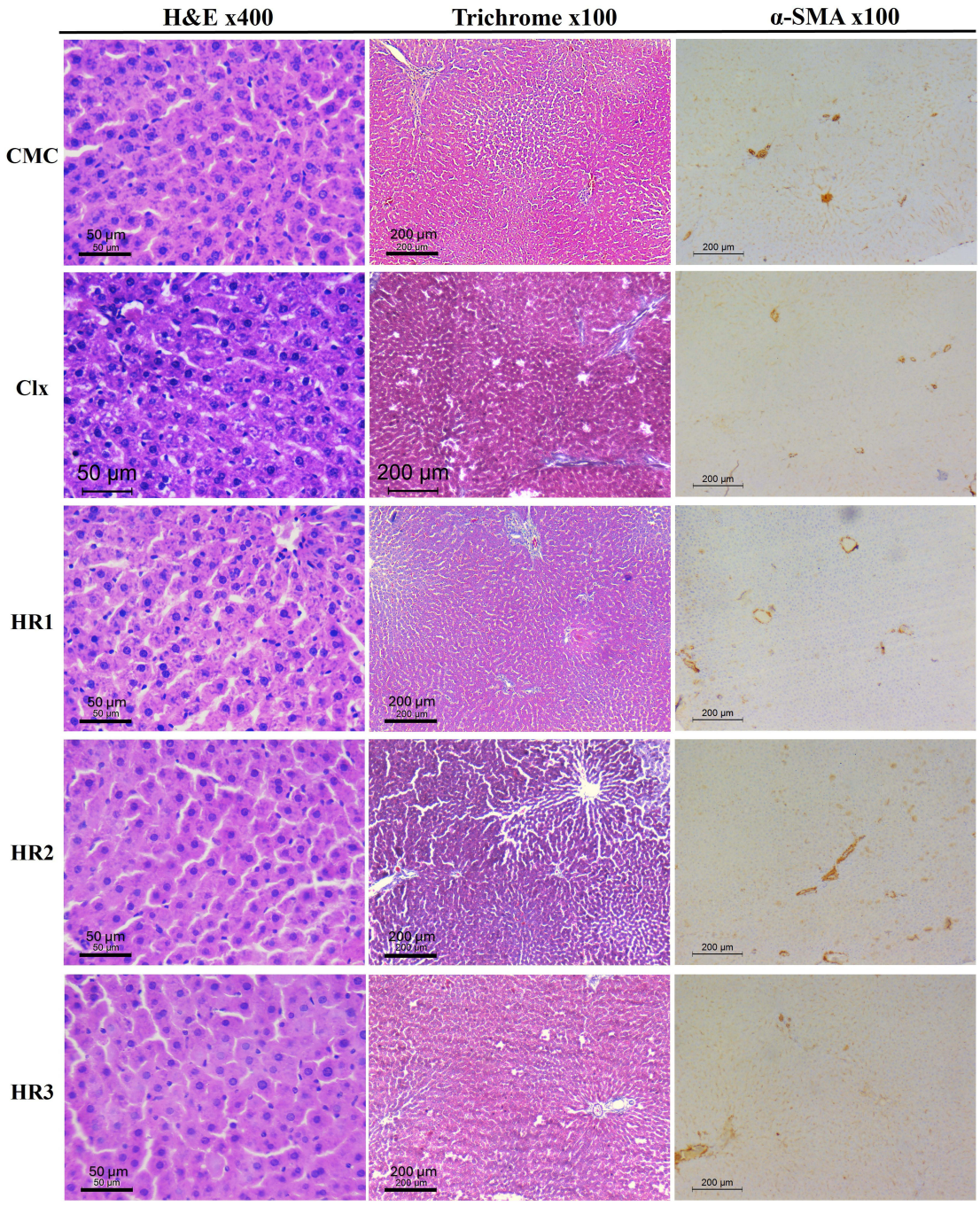

Figure 5 In vivo toxicity study. Effect of celecoxib and its bipyrazole congeners HR1-3 on liver architecture. The bipyrazoles showed normal histology as represented by H&E, Masson's trichrome, and immunohistochemical staining of α-smooth muscle actin (α-SMA).

Masson's trichrome staining highlighted that the fibrous septea in the model group was edematous showing lymphoplasmacytic infiltrates, denoting stage 4 liver fibrosis. On the contrary, the portal tracts of the control group appeared small, with scanty fibrous tissue around, pointing to zero liver fibrosis score. The treatment groups of celecoxib and the analogs **HR1-3** showed evident regression of fibrosis score (Figure 7). One way ANOVA statistical analysis was carried out based on the obtained fibrosis scores. The results revealed a significant decrease in fibrosis scores of the groups treated with celecoxib, as well as the compounds in question **HR1-3**. Among these, the fluorinated analog **HR3** displayed a superior fibrolytic effect to that of celecoxib, whereas the analogs **HR1** and **HR2** were almost equipotent with the reference drug (Figure 8A).

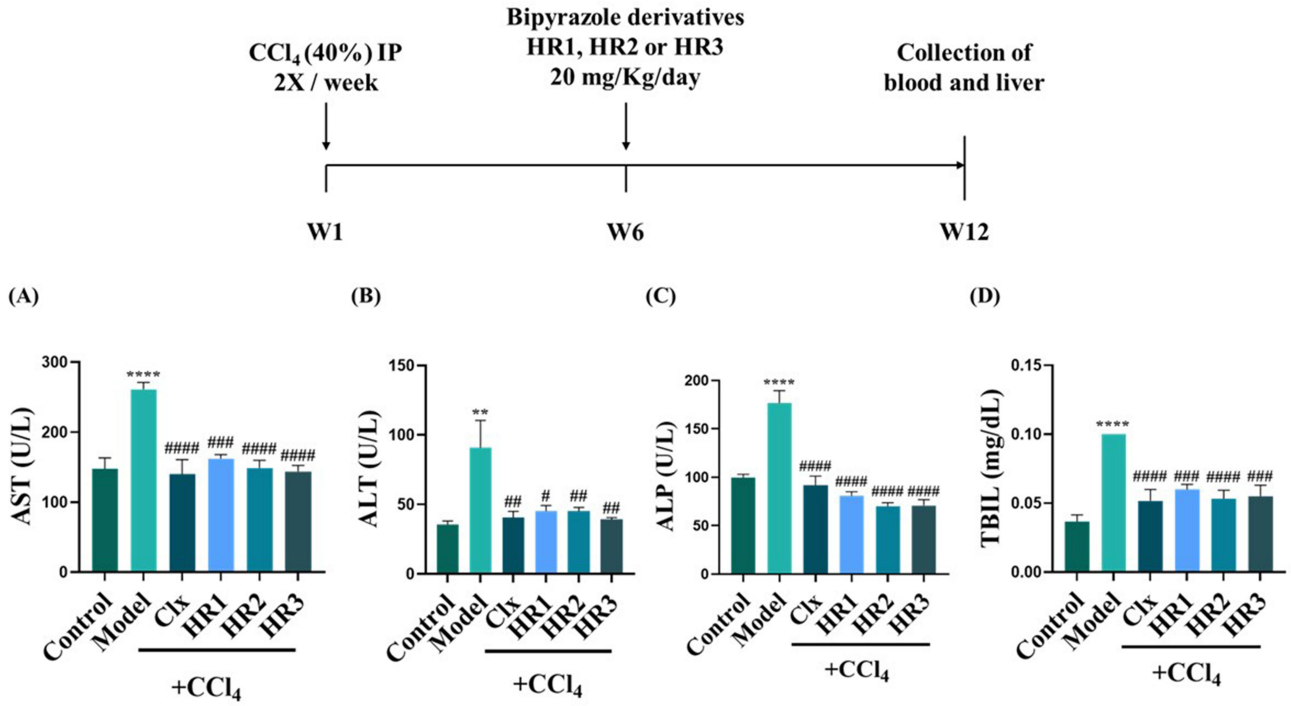

Figure 6 Liver biomarkers in rats with CCl_4-induced liver fibrosis and different treatment groups. **(A)** AST (U/L), **(B)** ALT (U/L), **(C)** ALP (U/L), and **(D)** TBIL (mg/dL).
Notes: The data are expressed by bar graph and the values are presented as mean ± SEM; n = 5. ** (P ≤ 0.01) and **** (P ≤ 0.0001) compared to control group. # (P ≤ 0.05), ## (P ≤ 0.01), ### (P ≤ 0.001) and ##### (P ≤ 0.0001) compared to the fibrosis model group.

Moreover, the fibrosis model group displayed wide areas of α-SMA immunopositive areas, where the calculated percentage of α-SMA touched 50%. Meanwhile, the control group showed very small α-SMA-positive areas. Different groups treated with either celecoxib or any of the three tested compounds **HR1-3** showed a significant decline of the α-SMA % indicating the resolution of liver fibrosis (Figure 7). In particular, the fluorinated analog **HR3** exerted the best fibrosis-resolving effect as reflected from the obviously low α-SMA % obtained (14.5%). Statistical analysis of the data obtained revealed the significant difference in the α-SMA-positive areas between the model and control groups. Moreover, the groups treated with compounds **HR1-3** displayed a remarkable reduction in the α-SMA deposition, which was nearly comparable to that of celecoxib (Figure 8B).

HR1-3 Downregulated TGFβ-1 and Reversed Tissue Remodeling in Induced Liver Fibrosis

The expression levels of TGF-β1 were measured as it plays a key role in liver fibrosis via inducing matrix production. The results revealed a remarkable increase in the expression of TGF-β1 in the fibrosis model. Interestingly, celecoxib and the three investigated drugs **HR1-3** displayed a significant reduction in the expression of TGF- β1, specifically **HR3,** whereas **HR1** proved to be less potent than **HR2** and **HR3**. Nevertheless, all of the three tested compounds were more effective than celecoxib (Figure 9A).

Fibrogenesis and regression of liver fibrosis have been associated with dynamic changes in MMP and TIMPs levels. In this work, upon measuring the levels of TIMP-1 and MMP-9, the results showed a significant increase in the levels of TIMP-1 in the case of the fibrosis model group in comparison to its levels in the control group. Statistical analysis also revealed a significant difference in all treatment groups, where the novel drugs (**HR1-3**) showed a comparable effect to that of celecoxib, which caused a decrease in TIMP-1 levels in liver tissues. The decrease in TIMP-1 levels was nearly equal to that presented by the control group (Figure 9B). On the other hand, MMP-9 was significantly upregulated in the model group and treatment with celecoxib and the three tested drugs

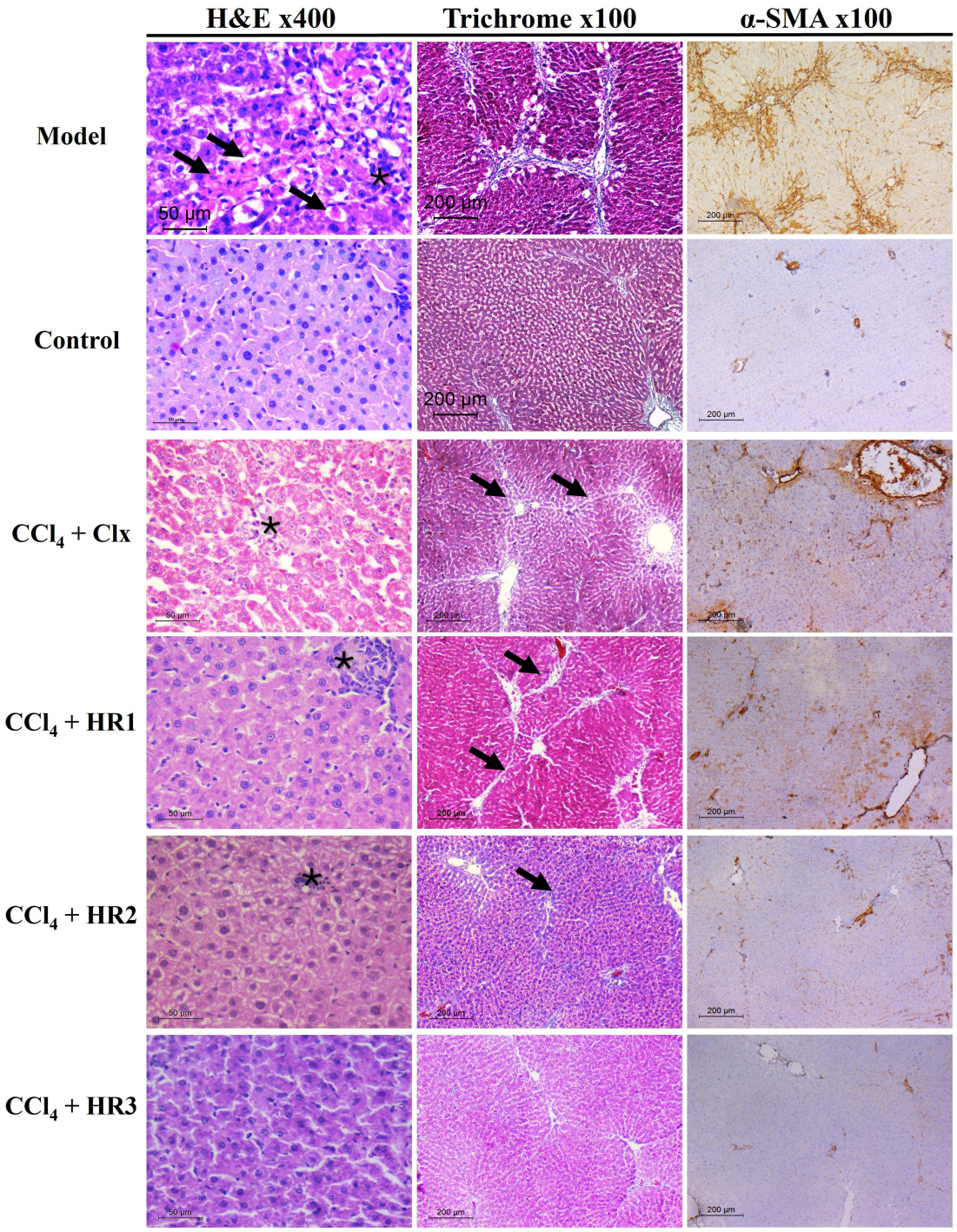

Figure 7 Microscopic analysis of liver tissues using different staining methods. H&E-stained sections of fibrosis model group showed evident degenerative changes in hepatocytes as Councilman bodies (arrows) and lobular inflammation (asterisk) (x400). The control group (oil + CMC) showed histologically free hepatocytes (x400). The treated groups (celecoxib and **HR1-3**) showed histologically free hepatocytes with only minimal inflammation (asterisk) (x400). Masson's trichrome stain of the model group showed lobular architecture separated by blue fibrous septea (x100) and minimal fibrous tissue around portal tracts (x100) in the control group. Restoration of normal lobular architecture with occasional fibrous septea (arrow) (x100) was seen in the treated groups. The immunostained liver biopsies showed wide areas of brown staining in fibrosis model group in contrast to the control group (IHC, x100). The staining of the different treated groups receiving celecoxib or **HR1-3** showed a decline in α-SMA % (IHC, x100).

reversed that upregulation. In particular, **HR2** and **HR3** caused a significant reduction in MMP-9 expression compared to the control group. Interestingly, the three drugs in question showed superior MMP-9 expression lowering effects as compared to standard celecoxib (Figure 9C).

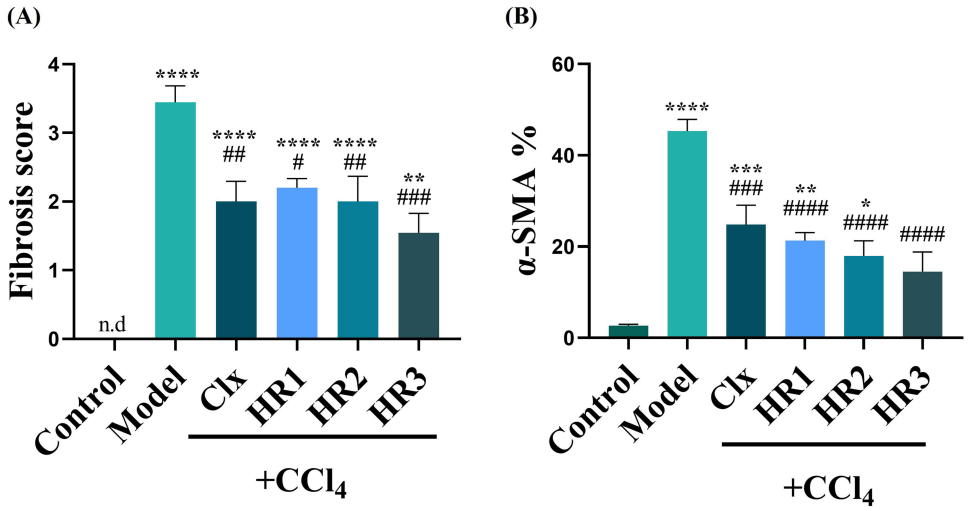

Figure 8 Effect of treatment with different compounds **HR1-3** on CCl_4-induced liver fibrosis induced model. **(A)** Fibrosis score (0–4) **(B)** α-SMA- positive area (%).
Notes: The data are expressed by bar graph and the values are presented as mean ± SEM; n = 5. * (P ≤ 0.05), ** (P ≤ 0.01), *** (P ≤ 0.001) and **** (P ≤ 0.0001) compared to control group. # (P ≤ 0.05), ## (P ≤ 0.01), ### (P ≤ 0.001) and ##### (P ≤ 0.0001) compared to the fibrosis model group.

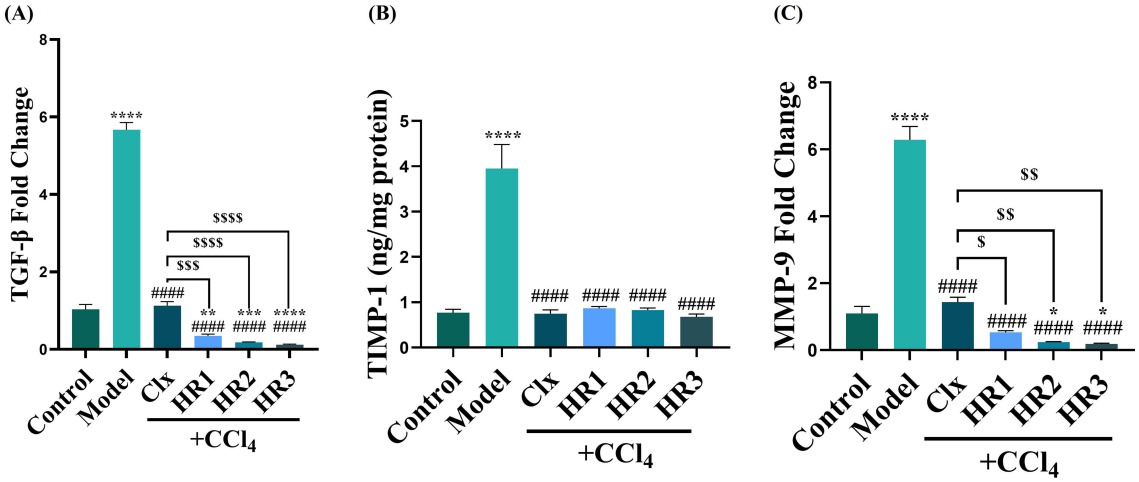

Figure 9 Impact of treatment with different compounds **HR1-3** on CCl_4-induced liver fibrosis on tissue remodeling. **(A)** Hepatic profibrogenic cytokine TGF-β1 mRNA levels of expression in liver fibrosis and treatment groups (fold change). **(B)** Hepatic TIMP-1 protein levels in tissue homogenates (ng/mg protein). **(C)** Hepatic mRNA expression levels of MMP-9 (fold change).
Notes: The data are expressed by bar graph and the values are presented as mean ± SEM; n = 5. * (P ≤ 0.05), ** (P ≤ 0.01), *** (P ≤ 0.001) and **** (P ≤ 0.0001) compared to control group. ##### (P ≤ 0.0001) compared to the fibrosis model group. $ (P ≤ 0.05), $$ (P ≤ 0.01), $$$ (P ≤ 0.001) and $$$$ (P ≤ 0.0001) compared to the CCl_4 + Clx group.

Antioxidant Potentials of HR1-3 in Liver Fibrosis Mitigation

Oxidative stress is a crucial factor in the development of liver fibrosis. In the present work, an increase in MDA levels was detected in the fibrosis model along with exhaustion of GSH, indicating the presence of oxidative stress due to fibrosis. Upon treatment with celecoxib and the three tested compounds **HR1-3**, the analog **HR3** proved to be a potential antioxidant candidate as its effect was either comparable or superior to that of celecoxib. Meanwhile, **HR2** was only able to alleviate the oxidative stress regarding GSH with no effect on MDA. However, **HR1** was not capable of exerting any significant antioxidant effects (Figures 10A and B).

HR1-3 Reduced Proinflammatory Cytokines in Induced Liver Fibrosis

As inflammation is known to be one of the leading causes of liver fibrosis, it appeared plausible to measure contents and expression levels of some proinflammatory cytokines, in particular the TNF-α and IL-6. The fibrosed model displayed highly

https://doi.org/10.2147/DDDT.S512058

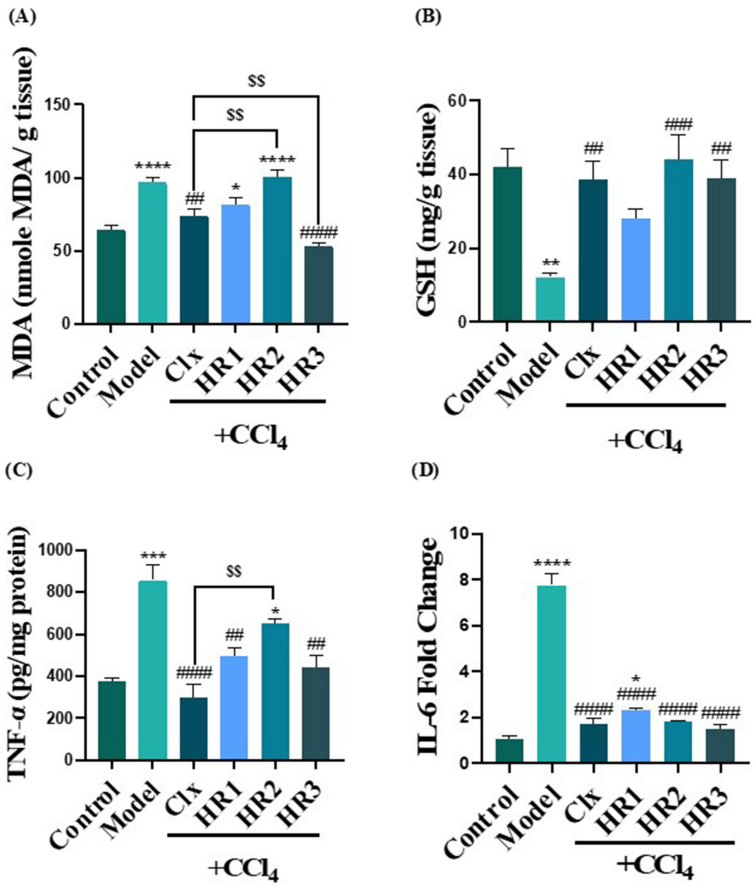

Figure 10 Oxidative stress and proinflammatory biomarkers in liver tissue homogenates of fibrosed and treated groups. **(A)** MDA content (nmol/mL). **(B)** GSH (mg/g tissue). **(C)** Liver TNF-α content (pg/mg protein). **(D)** liver mRNA expression of IL-6 (fold change).

Notes: The data are expressed by bar graph and the values are presented as mean ± SEM; n = 5. * (P ≤ 0.05), ** (P ≤ 0.01), *** (P≤0.001) and **** (P ≤ 0.0001) compared to control group. ## (P ≤ 0.01), ### (P ≤ 0.001) and ##### (P ≤ 0.0001) compared to the fibrosis model group. $$ (P ≤ 0.01), compared to the CCl_4 + Clx group.

elevated TNF-α protein levels, in addition to the overexpression of IL-6 gene confirming that inflammation is strongly contributing to liver fibrosis. Meanwhile, celecoxib exhibited a significantly superior effect in lowering TNF-α levels compared to the tested compounds **HR1** and **HR3**. However, the decrease in the TNF-α levels displayed by the analog **HR2** was statistically insignificant. On the other hand, **HR1-3** showed comparable effects to celecoxib in lowering IL-6 expression; however, none of them were able to achieve equivalent levels to that in control group (Figures 10C and D).

Molecular Modelling Studies for the Prediction of Possible Mechanism of Action

Docking to TNF-α Active Site

Based on the pre-mentioned experimental findings proving that celecoxib (the reference standard drug implemented in the present work) and the three investigated bipyrazoles **HR1-3** exhibited reliable TNF-α lowering effects, it was thought worthwhile to carry out an in silico molecular docking study to estimate their binding mode and the possible molecular interactions with the active site of the TNF-α molecule. Molecular Operating Environment (MOE) version 2016.0802 was utilized for docking, whereas the X-ray structure of the TNF-α molecule with its co-crystallized ligand (307) was retrieved from the RCSB Protein Data Bank PDB (ID: 2AZ5).[56] Re-docking of (307) in the TNF-α active site validated the docking protocol with root mean square deviation (RMSD) of 1.98 Å between the docked pose and the co-crystallized ligand and with binding energy score of −5.42 kcal/mol. This RMSD score assured the validity of the used docking protocol being less than 2 Å.[53]

The results of the docking study indicated that the three investigated bipyrazoles **HR1-3** were flexibly docked, well occupied, and positioned onto the active site of TNF-α. The analogs **HR1-3** recorded good binding affinity energies

(−5.25, −5.31 and −5.73 Kcal/mol, respectively), nearly equivalent to that of the co-crystallized ligand (307) (−5.42 kcal/mol), however, much better than that displayed by the reference drug celecoxib (−4.61 kcal/mol). The overall binding patterns of celecoxib and the analogs **HR1-3** were found to be related to those observed with the co-crystallized ligand with some differences, and the docking poses were chosen according to the most favorable binding interactions.

As can be seen from both the 2D and 3D docking poses in the active site of TNF-α (2AZ5), celecoxib (Figure 11B and Figure 12B) and the three analogs **HR1-3** (Figure 11 and Figure 12) were engaged in several molecular interactions with a binding pattern similar to that displayed by the co-crystallized ligand (307) (Figure 11A and Figure 12A). For instance, they exhibited the same π hydrophobic interactions presented by the co-crystallized ligand (307) towards the amino acid residues Try119 and Tyr59. Regarding the binding mode of celecoxib, the NH_2 of the aminosulfonyl group formed a H-bond with Tyr151 and as H-bond donor. Whereas, **HR1-3** could display several π-H interactions involving the antipyrine-phenyl, 4-substituted phenyl moieties with Pro117and Ile118 amino acid residues.

Docking to TGF-β Active Site

It was thought meaningful to extend the in silico molecular docking study to estimate the binding mode and the possible molecular interactions with the active site of the TGF-β molecule, based on the previously mentioned findings indicating the reliable TGF-β lowering effects of celecoxib and the three investigated bipyrazoles **HR1-3**. Molecular Operating Environment (MOE) version 2016.0802 was utilized for docking, whereas the X-ray structure of the TGF-β molecule with its pyrazole co-crystallized ligand was retrieved from the RCSB Protein Data Bank PDB (ID: 1JVY).[57] Re-docking of the pyrazole co-crystallized ligand in the TGF-β active site validated the docking protocol with root mean square deviation (RMSD) of 0.81 Å between the docked pose and the co-crystallized ligand and with binding energy score of −8.14 kcal/mol. This RMSD score assured the validity of the used docking protocol being less than 2 Å.[53]

The results of the docking study indicated that the three investigated bipyrazoles **HR1-3** were flexibly docked, well occupied, and positioned onto the active site of TGF-β. **HR1-3** recorded good binding affinity energies (−8.47, −8.72 and −8.94 Kcal/mol, respectively), nearly equivalent to that of the co-crystallized ligand (−8.14 kcal/mol), however, much better than that displayed by the reference drug celecoxib (−6.97 kcal/mol).

According to the 2D and 3D docking poses in active site of TGF-β (1JVY), celecoxib (Figure 13B and Figure 14B) and the three analogs **HR1-3** (Figure 13 and Figure 14) revealed almost the same π hydrophobic interactions presented by the pyrazole co-crystallized ligand (Figure 13A and Figure 14A) towards the amino acid residue Lys 232. Meanwhile, **HR1-3** could display extra π-H interactions involving the antipyrine pyrazole ring and the 4-substituted phenyl moieties with Val219, Lys213 and Gly285 amino acid residues. Regarding the ability of the investigated analogs to participate in H-bonding, the 2D and 3D poses of the analog **HR1** revealed the formation of two direct H-bonds between carboxamide-N and aniline-N with Ile211 residue as H-bond acceptors. Furthermore, the analog **HR2** showed the existence of one H-bond between the thiol group and Asp281 as H-bond donor, beside another three H-bonds between the antipyrine-*O* atom and the nitro 2*O* atoms, with Lys213, Lys232 and Asp351, respectively, as H-acceptors. Concerning the fluorinated analog **HR3**, it could form a H-bond with Ile211 as H-bond donor, together with another H-bond with His283 as H-acceptor. It is to be noted that the aminosulfonyl group in celecoxib formed a water-mediated H-bond with Tyr249, Asp351 and Glu245 through the water molecule W1001, in addition to a second H-bond between fluorine and His283 residue as H-bond acceptors.

In silico Prediction of the Physicochemical Properties, Drug-Likeness, Pharmacokinetics, and Toxicity Profile

Early computation and determination of the physicochemical properties and the pharmacokinetics of new drug candidates is of paramount importance in the lead optimization and drug development process.[58] Accordingly, in silico physicochemical properties, drug likeness and pharmacokinetic parameters of the investigated compounds **HR1-3** were predicted using web-based applications such as Molinspiration, Pre-ADMET, and Osiris property explorer software (previously mentioned in the materials and methods section). These parameters would show the behavior of the drugs in a living system including bioavailability, affinity to proteins, membrane transport characters, metabolic stability, and toxicity. In the light of Lipinski's rule of five (RO5)[59] and Veber's criteria,[60] it was found that the three investigated compounds

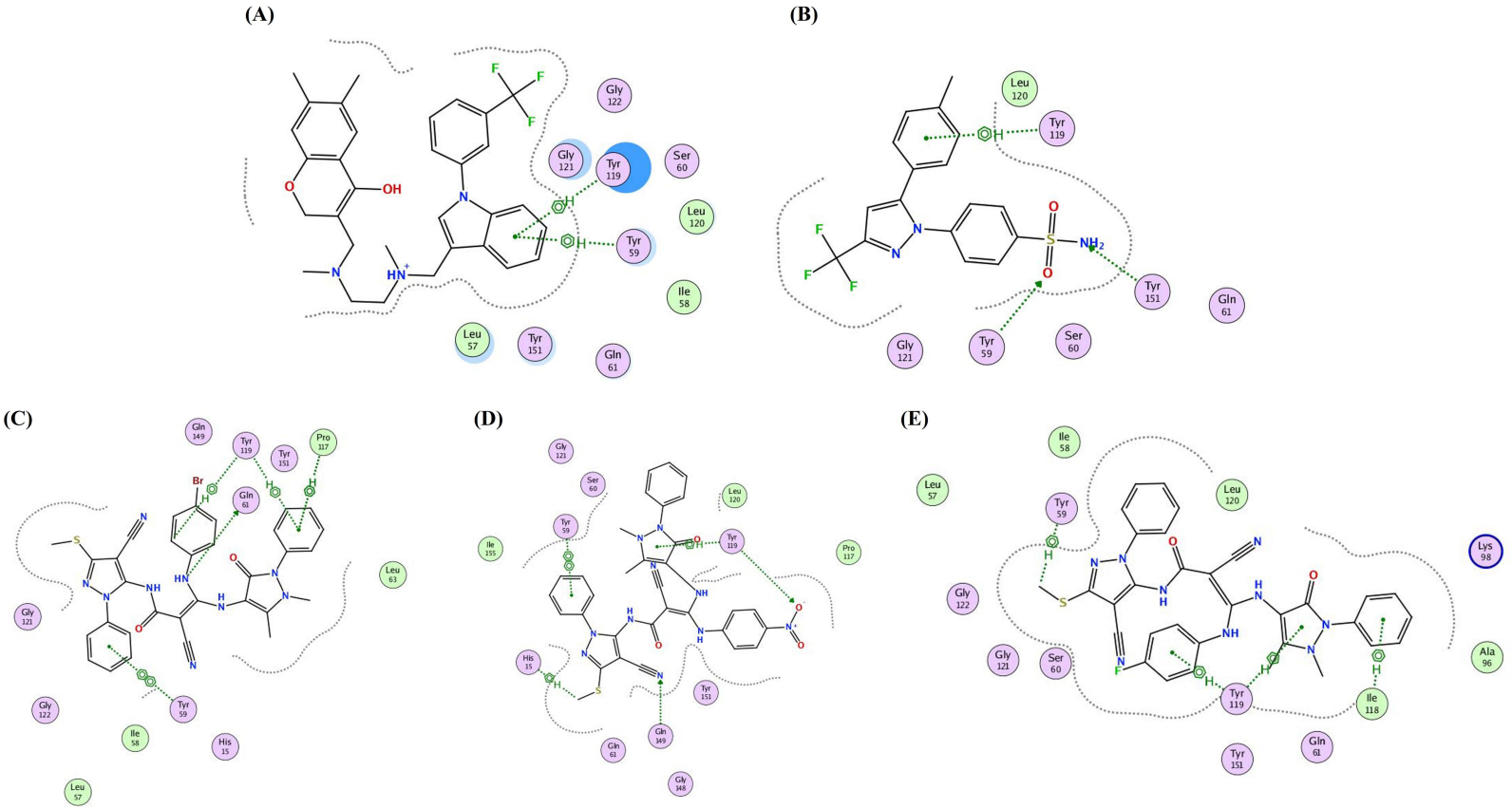

Figure 11 2D presentation of the most favorable binding poses and ligand interactions into the active site of TNF-α (PDB: 2AZ5) **(A)** Co-crystallized ligand. **(B)** Celecoxib. **(C)** analog **HR1. (D)** analog **HR2. (E)** analog **HR3**.

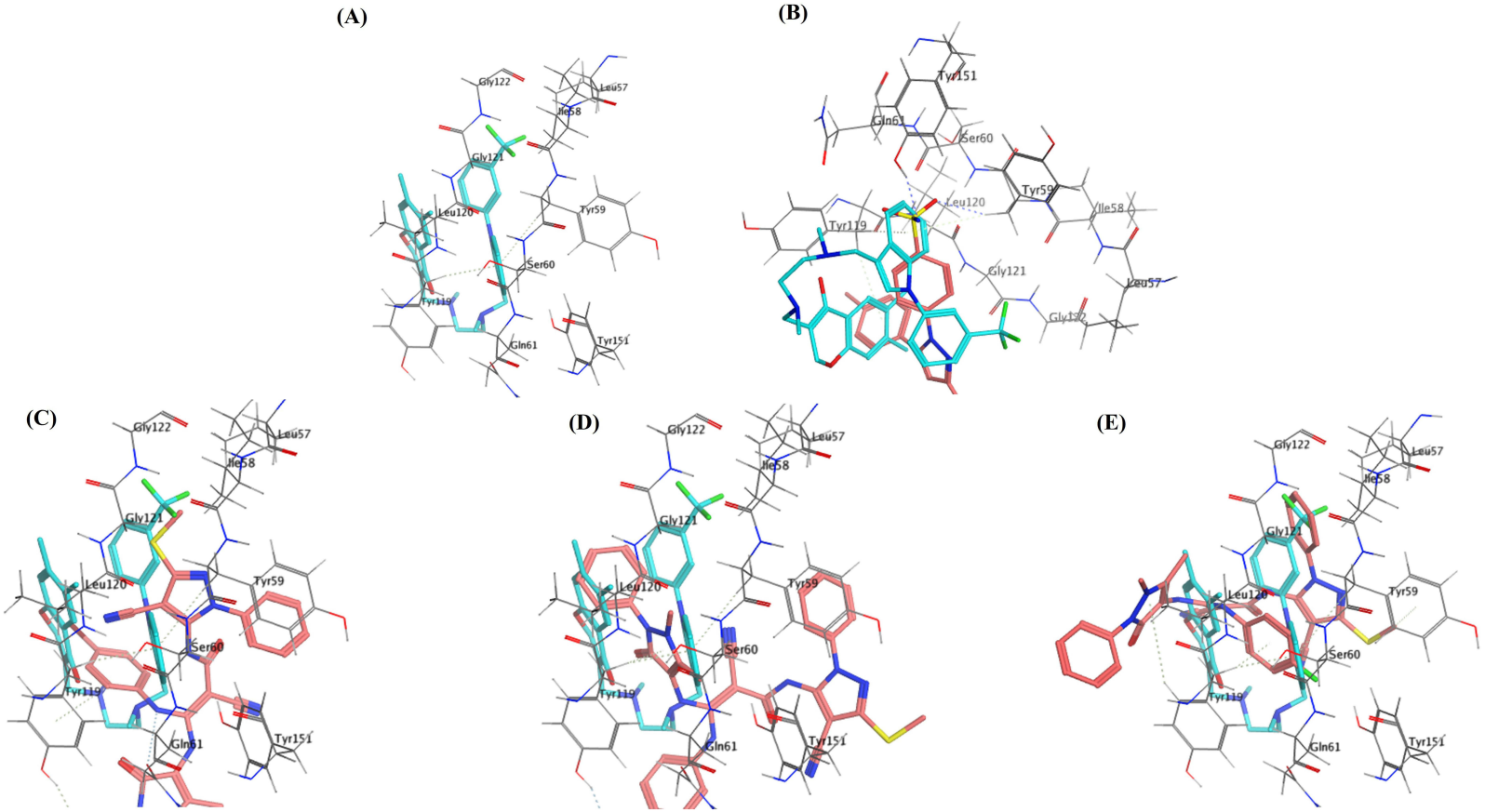

Figure 12 3D presentation of the docking and binding patterns into the active site of TNF-α (PDB: 2AZ5) **(A)** Co-crystallized ligand. **(B)** Celecoxib (in pink) and its overlay over the co-crystallized ligand (in cyan). **(C)** analog **HR1** (in pink) and its overlay over the co-crystallized ligand (in cyan). **(D)** analog **HR2** (in pink) and its overlay over the co-crystallized ligand (in cyan). **(E)** analog **HR3** (in pink) and its overlay over the co-crystallized ligand (in cyan).

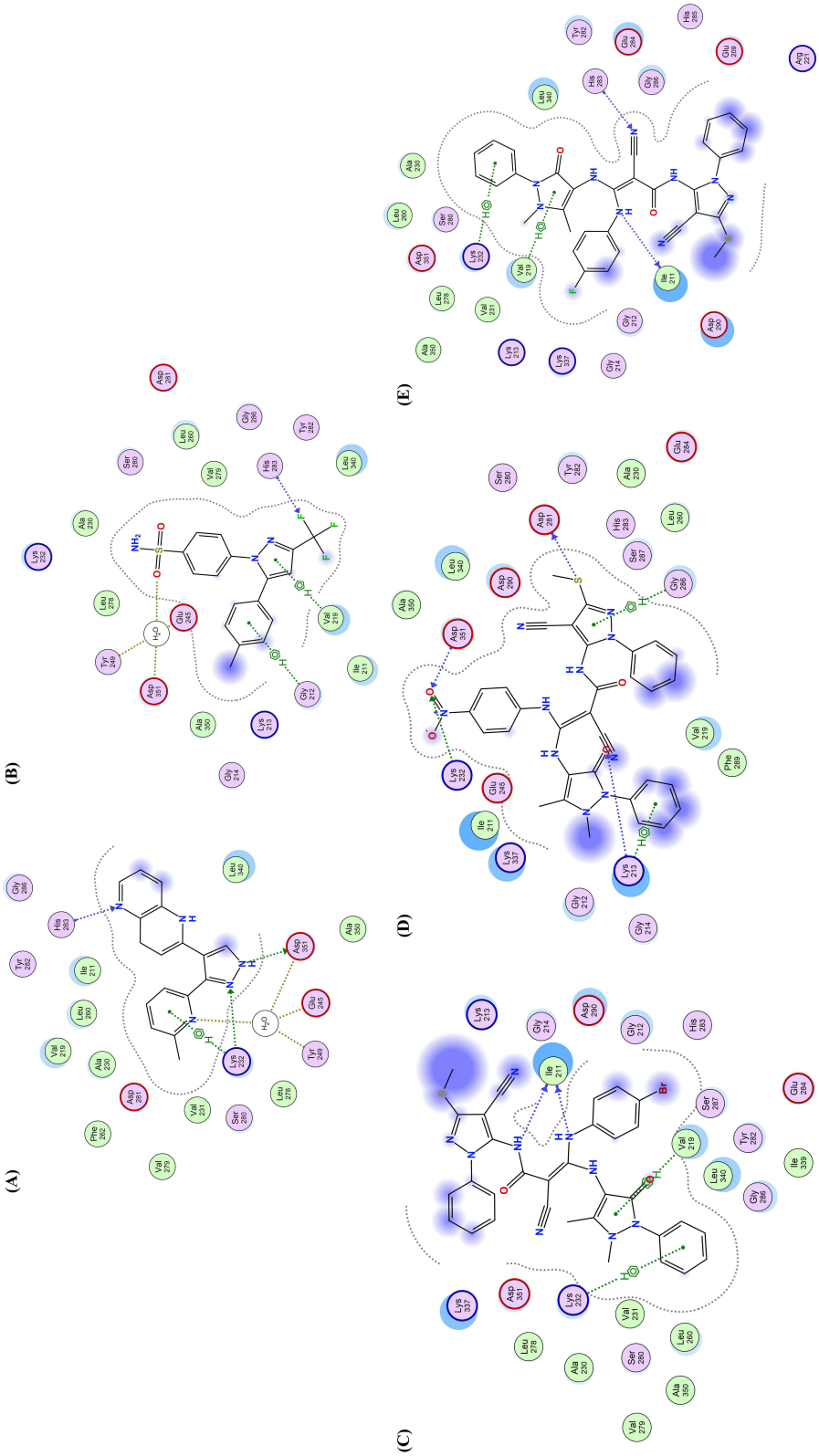

Figure 13 2D presentation of the most favorable binding poses and ligand interactions into the active site of TGF-β (PDB: 1VJY) **(A)** Co-crystallized ligand. **(B)** Celecoxib. **(C)** analog **HR1**. **(D)** analog **HR2**. **(E)** analog **HR3**.

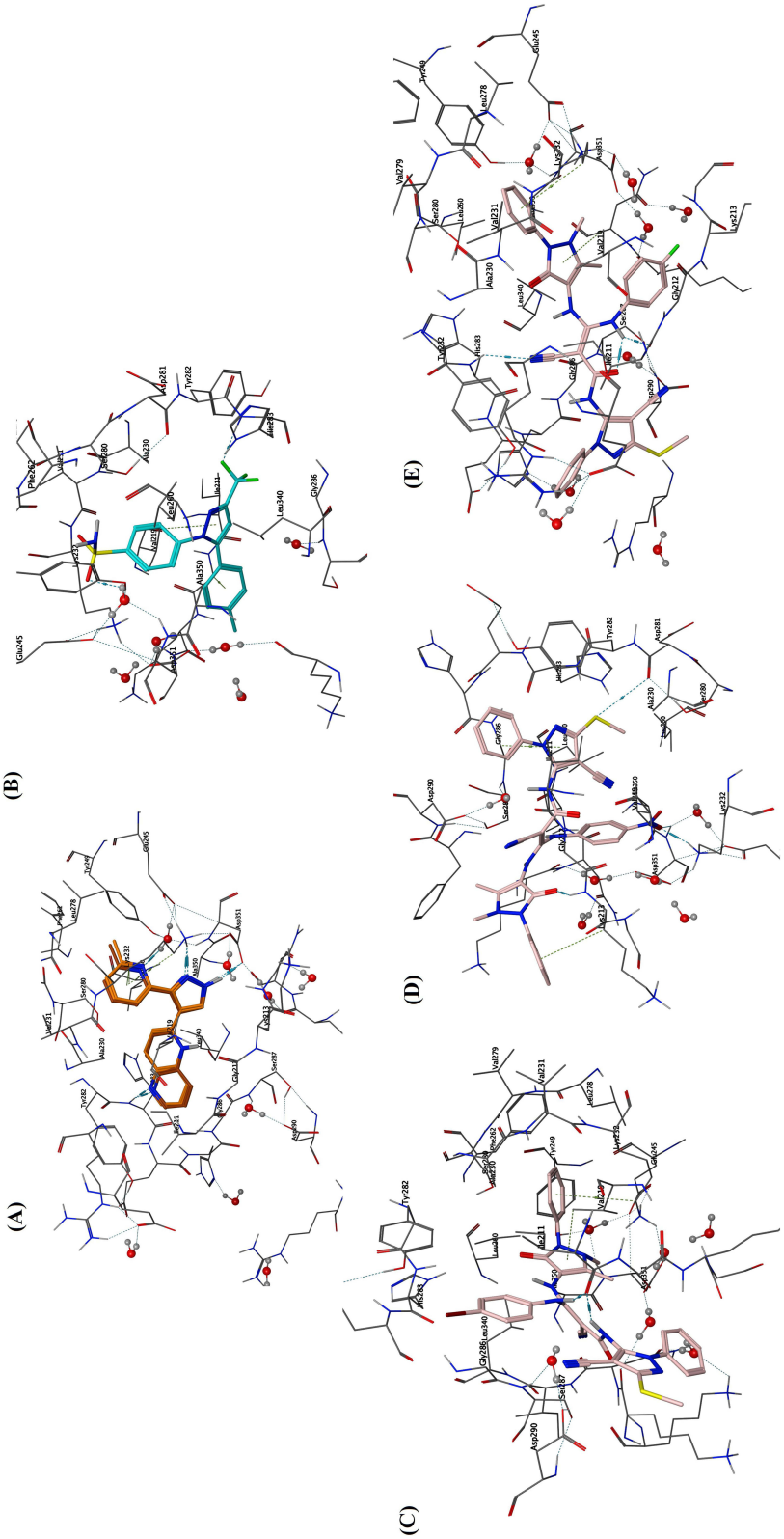

Figure 14 3D presentation of the docking and binding patterns into the active site of TGF-β (PDB: 1VJY) **(A)** Co-crystallized ligand. **(B)** Celecoxib (in cyan). **(C)** Analog **HR1** (in pink). **(D)** Analog **HR2** (in pink). **(E)** Analog **HR3** (in pink).

https://doi.org/10.2147/DDDT.S512058

violate two criteria of RO5, where MW range 619.69–680.59 (>500) and HBA range 11–14 (>10), whereas they displayed acceptable ranges of HBD (3) and logP values (2.99–3.84). Moreover, all the tested compounds violate one criteria of Veber's rule displaying topological polar surface area (TPSA) range of 145.50–191.32 Å² (>140 Å²) and nROTB values of 9–10 (≤10). Furthermore, all the investigated compounds exhibited a percentage of absorption (% ABS) range 42.99–58.80% and it is noted that the TPSA is inversely proportional to %ABS eg the analog **HR2** possesses the maximum TPSA (191.32 Å²), whereas its corresponding %ABS was the least (42.99%). Regarding the drug-likeness score values,[61] the results indicated that all the evaluated compounds gave positive values lying between 0.05 and 0.1 (Table 3). On the other hand, ADME properties were also predicted using Pre-ADMET software, and the value of each of the following parameters was calculated and compared with the optimal values: Caco-2 cell permeability coefficient (Permeability through cells derived from human colon adenocarcinoma), Madin-Darby canine kidney (MDCK) cell permeability coefficient, human intestinal absorption (HIA), blood brain barrier (BBB) coefficient, and plasma protein binding (PPB). As depicted in Table 3, the results showed that all three compounds **HR1-3** displayed moderate cell permeability in Caco-2 cell model (19.36–21.76 nm/sec) that lies within the acceptable range (4–70 nm/sec). Nevertheless, all of them displayed low permeability in MDCK cell model of 0.04 nm/sec in relation to the acceptable range (25–500 nm/sec). Regarding the HIA, the investigated compounds were well absorbed, exhibiting high HIA values (92.50–95.30%). Meanwhile, the three compounds showed low permeability to blood brain barrier (0.06–0.08) (<0.1). Furthermore, the analog **HR2** was found to be strongly bound to plasma proteins (>90%), whereas the analogs **HR1** and **HR3** showed poorer binding profile (<90%).[18,63]

Discussion

Liver fibrosis is still considered as a life-threatening disease that imposes a major impact on the morbidity and mortality of hepatic patients worldwide. It is a natural immune response describing a highly conserved and coordinated wound healing process that aims to maintain the integrity of liver through simultaneous inflammation, remodeling, and tissue repair.[6,64] Fibrosis is usually accompanied by remodeling of the hepatic and vascular architecture with the formation of septea and regenerative nodules. In addition, it could induce abnormal continuation of connective tissue production and extracellular matrix (ECM) deposition due to an imbalance between augmented synthesis and the decreased degradation.[9,65] This leads to the formation of parenchymal scars, which are initially deposited in portal tracts and/or in the lobule depending on the injury pattern.[66,67] Hepatic reparative mechanisms are generally attributed to increased degradation of collagen, loss of TGF-β signaling, and reduction in TIMP-1 expression, which in turn allows MMPs to degrade collagen types I and III.[12,17]

Liver fibrosis is an intricate process involving liver parenchymal and non-parenchymal cells including immune cells that have dual function in the progression and reversal of liver fibrosis.[9,68,69] Collectively, the cornerstones of the resolution of fibrosis are dependent on four fundamental points: (a) cessation of the main cause of chronic liver injury; (b) reversal of myofibroblasts from an activated to a non-activated condition and/or their removal; (c) degradation of the unnecessary ECM, and (d) alteration of proinflammatory environment to a healing one. Finally, the removal of aHSCs could be attained by apoptosis or senescence.[9,70,71]

CCl_4-induced liver fibrosis models are well known to mimic clinical liver fibrosis in humans,[72] where liver biopsy is considered as a golden standard method to diagnose liver fibrosis.[73] The changes in liver histology in our study were in agreement with a published work reporting the ability of CCl_4 to cause a serious distortion of the hepatic architecture exemplified by portal and lobular inflammation, bridging fibrosis, as well as early cirrhotic nodule formation.[74] Moreover, extensive deposition of α-SMA was determined in our studies, which goes in hand with the results mentioned in a previous study, where α-SMA expression was increased in CCl_4 hepatic fibrosis model.[75]

Here, it should be mentioned that the control group showed normal α-SMA deposition and architecture, which could be correlated with normal liver enzyme levels (AST, ALT and ALP). Conversely, the fibrosis model demonstrated a substantial rise in the three liver enzymes in response to liver fibrosis, which was detected by histology and immunohistochemistry. While AST and ALP are not liver-specific biomarkers, elevation of ALT levels could indicate a chronic liver disease. Collectively, treatment with celecoxib and its related compounds (**HR1-3**) caused a significant decline in fibrosis score as well as α-SMA%, which was validated by the reduction in the liver enzyme panel.

Table 3 In silico Prediction of the Physicochemical Properties, Drug-Likeness and Pharmacokinetics of Compounds HR1-3

	HR 1	HR 2	HR 3	Celecoxib
LogP[a]	3.84	2.99	3.19	3.61
M.Wt[b]	680.59	646.69	619.69	381.38
HBA[c]	11	14	11	5
HBD[d]	3	3	3	2
Lipinski's violation[e]	2	2	2	0
NROTB[f]	9	10	9	4
TPSA[g]	145.50	191.32	145.50	77.99
%ABS[h]	58.80	42.99	58.80	82.09
Volume[i]	543.63	549.08	530.68	298.65
Drug-likeness score	0.08	0.05	0.1	0.37
Caco-2[j]	21.76	19.36	21.60	0.50
MDCK[k]	0.04	0.04	0.04	45.05
HIA[l]	95.30	92.50	94.66	96.69
BBB[m]	0.06	0.08	0.06	0.03
PPB[n]	86.71	90.15	88.20	91.08

Notes: [a] **LogP**, n-Octanol and water partition coefficient; [b] **M.Wt**, Molecular weight; [c] **HBA**, Number of H-bond acceptors; [d] **HBD**, Number of H-bond donors; [e] **Lipinski's violation**, Lipinski's rule of 5 violations (log P ≤ 5, M.Wt. ≤ 500, HBA ≤ 10 and HBD ≤ 5); [f] **NROTB**, Number of rotatable bonds (Veber's criteria ≤ 10); [g] **TPSA**, Topological polar surface area (Veber's criteria ≤ 140 Å^2); [h] **%ABS**, Percentage of absorption = 109 – (0.345*TPSA); [i] **Volume**, Molecular volume; [j] **Caco-2**, Permeability through human colon adenocarcinoma cells.; Caco2 values < 4 nm/sec (low permeability), values from 4 to 70 nm/sec (medium permeability) and values > 70 nm/sec (high permeability); [k] **MDCK**, Permeability through Madin-Darby canine kidney cells; MDCK values < 25 nm/sec (low permeability), values from 25 to 500 nm/sec (medium permeability) and values > 500 nm/sec (high permeability);. [l] **HIA**, Human intestinal absorption percentage; HIA values from 0 to 20% (poorly absorbed), values from 20 to 70% (moderately absorbed) and values from 70 to 100% (well absorbed); [m] **BBB**, Blood brain barrier penetration coefficient; BBB values < 0.1 (low CNS penetration), values from 0.1 to 2 (medium CNS absorption) and values > 2 (high CNS absorption); [n] **PPB**, Plasma protein binding; PPB values < 90% (poorly bound) and > 90% (strongly bound).

In 1965, Comporti et al and Ghoshal et al[76,77] were the first to report the association between ROS and liver fibrosis induced by CCl_4 through lipid peroxidation. Oxidative stress is known to be implicated in liver injuries and fibrosis, caused by alcohol intake, iron overload, and HCV infection.[78] Glutathione (γ-glutamyl-cysteinyl-glycine) is a vital and widely present intra-cellular tripeptide that plays a variety of physiological roles,[79] and is considered as the most important antioxidant in the mammalian liver.[80] Normally, GSH is highly concentrated in cellular systems, and is essential in the detoxification of a wide range of compounds.[81] MDA is another oxidative stress biomarker as it is produced among the terminal products of the polyunsaturated fatty acids peroxidation process in cells. MDA is over-produced in response to increased free radicals' production.[82] Our results are in concordance with published results reporting the unfavorable effect of CCl_4 on GSH levels, where its levels were diminished due to increased oxidative stress.[83] Also, our findings agreed with a study stating that MDA is a part of the body's antioxidant defense system and can reflect the body's antioxidant capability. The increasing levels of MDA are attributed to the oxidative stress resulting from the effect of CCl_4-induced liver fibrosis.[75]

The inflammatory markers TNF-α and IL-6 are known to be pleiotropic cytokines released by different types of immune cells eg macrophages and monocytes. They can induce multiple signaling routes that are linked to the pathogenesis of chronic liver inflammation causing fibrosis.[84,85] Literature findings have emphasized that CCl_4 rat liver fibrosis model is accompanied with upregulation of TNF-α in addition to elevated IL-6 levels.[75,86,87] Our results showed elevated expression levels of MMP-9 gene as well as a rise in TIMP-1 protein levels. Such effects were highlighted by Hafez et al.[88]

TGF-β1 is one of the most important cytokines leading to liver fibrosis. It plays an important role as a mediator of ECM deposition by regulating the expression of collagen type I and fibronectin causing an increase in ECM production.[25] Its levels were elevated in the CCl_4 fibrosis model, which is consistent with the results obtained from H&E and trichrome staining, and this was in concordance with the reported CCl_4 effect on TGF-β1 levels.[25,75]

Celecoxib (a selective COX-2 inhibitor) has been repurposed as a potential antifibrotic, fibrolytic, and hepatoprotective agent in some chronic liver fibrosis models (CCl_4, TAA and BDL models). Our results are in concordance with studies that had addressed its ability to reverse liver fibrosis. Those studies clarified the capability of celecoxib to significantly lower the hepatic ECM deposition, as well as mitigating the cirrhotic lesions in many induced liver fibrosis models either utilizing TAA or by Bile duct ligation (BDL).[23,24,26,27] On the other hand, another study conducted by Hui et al, showed that celecoxib exacerbated liver fibrosis in rats induced by CCl_4 or TAA. However, the doses used there were different than that employed in this study as they used 0.2 mL/100 g body weight of CCl_4 in olive oil (1:1), whereas in this study 40% CCl_4 in corn oil with a dose 0.2 mL/100 g bodyweight was used. In addition, Hui et al also used a lower dose of celecoxib (15 mg/Kg) which might explain the difference in response.[74] A published study confirmed that treatment of the TAA-induced rat liver fibrosis model with celecoxib resulted in the inhibition or even total loss of the mesenchymal biomarker α-SMA. This fact implies that celecoxib possesses the potential to reverse the EMT process in hepatocytes.[11] Interestingly, Gao et al reported the ability of celecoxib to decrease the upregulated expression of α-SMA in a liver fibrosis model at the same dose employed in the current study.[23] Moreover, the celecoxib treatment group's results were in synchronization with a previously published report denoting the relationship between celecoxib's antioxidant potential and its ability to lower the elevated MDA levels as well as elevate GSH levels in CCl_4 rat model of liver fibrosis.[25] Wen et al reported the effect of celecoxib on TAA-induced liver fibrosis. Celecoxib was able to downregulate the levels of TNF-α, IL-6 and MMP-9.[11] Our results are also in alignment with a previously published study that stated that CCl_4 increased TIMP-1 levels in the rat model, whereas celecoxib did not upregulate its level and that TGF-β1 mRNA was significantly diminished by celecoxib treatment of fibrosis in TAA and BDL induced liver fibrosis.[24,74,89]

Collectively, the objective of the present study is to discover a non-invasive treatment for liver fibrosis through investigating the possible ability of three celecoxib-related bipyrazole compounds **HR1-3** carrying different substituents (Br, NO_2 and F, respectively) to reverse chemically induced liver fibrosis in rats using CCl_4. The results of the histopathological, immunohistochemical, biochemical and biomolecular studies revealed that the fluorinated analog **HR3** (R = F) was stemmed as the most active member as compared to celecoxib, owing to its distinctive results obtained from the histopathological and immunohistochemical tests, beside its antioxidant potential reflected by its significant action on GSH and MDA levels. In addition, it showed reliable effects against some biomarkers, namely, TNF-α, Il-6, MMP-9, TIMP-1 and TGF-β1. Furthermore, bioactivity of the nitro derivative **HR2** (R = NO_2) was remarkably less than the fluorinated congener **HR3** in most of the employed investigations. However, it displayed some noticeable activities in the histopathological and immunohistochemical tests, and could successfully reduce the IL-6, MMP-9, TIMP-1 and TGF-β1 levels, and showed a satisfactory antioxidant effect via elevating the GSH level. Meanwhile, except for its moderate effects on the TNF-α, IL-6, MMP-9 and TGF-β1 levels, as well as the histopathological and immunohistochemical tests, the brominated derivative **HR1** (R = Br) proved to be the least active member in this series. It is to be noted that, all the investigated compounds **HR1-3** were effectively able to lower the elevated serum levels of the indirect biomarkers of liver fibrosis such as AST, ALT, ALP and TBIL, regardless of the type of substituent. Nevertheless, the toxicity study of the three tested compounds proved their safety with regard to both liver and kidney functions. Interestingly, the in silico molecular modeling studies were in harmony with the above-mentioned findings, where the docking order of the investigated compounds into the active sites of both TNF-α and TGF-β followed the order **HR3** > **HR2** > **HR1**, with binding scores comparable to that of their co-crystallized ligands. The distinctive bioactivity displayed by the fluorinated analog **HR3** could be justified by the well-documented facts emphasizing the role of the fluorine atom substituent in medicinal chemistry. Sterically, fluorine atom is the second smallest substitute after hydrogen at receptors and enzyme active sites. Owing to the electron-rich character of fluorine and the strong nature of the C-F bond compared to the C-H bond, it could form strong hydrogen bonds. The presence of a fluorine substituent usually increases drug's lipophilicity and consequently improves its absorption and penetrability through different biological barriers, which eventually would optimize the expected pharmacological properties.[90] Whereas, in the analog **HR2**, the nitro group is an electron-withdrawing function

where the nitrogen atom is deprived of the lone pair of electrons, and hence it is positively charged. As a result, the nitro group could alter the polarity and electronic properties of the bearing molecules, hence affecting their pharmacokinetics and pharmacodynamics.[91] On the other hand, as shown by the analog **HR1**, the bromo substituent was the least favorable one. Although the bromine is a highly electronegative atom that would confer acceptable lipophilicity to the molecule, yet its large size (compared with the fluorine and chlorine relatives) imparts some steric hinderance to the molecule that would hamper its binding to the receptor or enzyme's active site.[92]

Conclusions

The current study investigated the potential capacity of three celecoxib-related bipyrazoles, **HR1-3**, to reverse chemically induced liver fibrosis in order to find a non-invasive therapy for liver fibrosis. Based on the results of the histopathological examination using H&E and Masson's trichrome staining and immunohistochemical testing for the quantification of α-SMA % of the isolated model rat livers, celecoxib and the investigated compounds **HR1-3** showed evident fibrolytic effects. Such effects were manifested as partial to total restoration of normal liver architecture in addition to a significant decline of the α-SMA % indicating the resolution of liver fibrosis in rats treated with CCl_4. The levels of MMP-9, TGF-β 1 and TIMP-1 significantly decreased in liver tissues of all treatment receiving groups (celecoxib and **HR1-3**). Celecoxib exhibited a significantly superior effect in lowering TNF-α levels, whereas all treatment modalities were equally effective in lowering IL-6 levels. Under oxidative stress, the treatment with celecoxib, **HR2** and **HR3** resulted in a significant rise in GSH levels. On the other hand, assessment of the liver's lipid peroxide levels revealed that celecoxib and only **HR3** could exert a significant lowering effect on MDA levels. Moreover, the analogs **HR1-3** were effectively able to lower the elevated serum levels of the indirect biomarkers of liver fibrosis, namely, AST, ALT, ALP and TBIL, with good liver and kidney safety profile. The results obtained from the in silico docking of **HR1-3** onto the active sites of TNF-α and TGF-β were concordant with their corresponding biological findings, following the activity order **HR3** > **HR2** > **HR1**, with binding scores comparable to that of their co-crystallized ligands. The predicted in silico physicochemical properties, drug likeness and pharmacokinetic parameters using web-based applications suggested the appropriateness of the investigated three drug candidates **HR 1–3** to act as drugs with acceptable pharmacokinetics. Depending on the obtained results, the fluorinated analog **HR3** could serve as a novel therapeutic candidate for the treatment of liver fibrosis that deserves further derivatizations and investigations.

Disclosure

The authors declare no conflicts of interest in this work.

References

1. Wynn T. Cellular and molecular mechanisms of fibrosis. *J Pathol*. 2008;214(2):199–210. doi:10.1002/path.2277
2. Aydın MM, Akçalı KC. Liver fibrosis. *Turk J Gastroenterol*. 2018;29(1):14–21. doi:10.5152/tjg.2018.17330
3. Schuppan D, Ashfaq-Khan M, Yang AT, Kim YO. Liver fibrosis: direct antifibrotic agents and targeted therapies. *Matrix Biol*. 2018;68:435–451. doi:10.1016/j.matbio.2018.04.006
4. Bodzin AS, Baker TB. Liver transplantation today: where we are now and where we are going. *Liver Transpl*. 2018;24(10):1470–1475. doi:10.1002/lt.25320
5. Wu BM, Liu JD, Li YH, Li J. Margatoxin mitigates CCl4 induced hepatic fibrosis in mice via macrophage polarization, cytokine secretion and STAT signaling. *Int J Mol Med*. 2020;45(1):103–114. doi:10.3892/ijmm.2019.4395
6. Li J, Zhao Y-R, Tian Z. Roles of hepatic stellate cells in acute liver failure: from the perspective of inflammation and fibrosis. *World J Hepatol*. 2019;11(5):412. doi:10.4254/wjh.v11.i5.412
7. Masola V, Carraro A, Granata S, et al.. In vitro effects of interleukin (IL)-1 beta inhibition on the epithelial-to-mesenchymal transition (EMT) of renal tubular and hepatic stellate cells. *J Transl Med*. 2019;17(1):1–11. doi:10.1186/s12967-019-1770-1
8. Koyama Y, Wang P, Liang S, et al.. Mesothelin/mucin 16 signaling in activated portal fibroblasts regulates cholestatic liver fibrosis. *J Clin Invest*. 2017;127(4):1254–1270. doi:10.1172/JCI88845
9. Zoubek ME, Trautwein C, Strnad P. Reversal of liver fibrosis: from fiction to reality. *Best Pract Res Clin Gastroenterol*. 2017;31(2):129–141. doi:10.1016/j.bpg.2017.04.005
10. Kisseleva T, Brenner D. Molecular and cellular mechanisms of liver fibrosis and its regression. *Nat Rev Gastroenterol Hepatol*. 2021;18(3):151–166.
11. Wen SL, Gao JH, Yang WJ, et al.. Celecoxib attenuates hepatic cirrhosis through inhibition of epithelial to mesenchymal transition of hepatocytes. *J Gastroenterol Hepatol*. 2014;29(11):1932–1942. doi:10.1111/jgh.12641

12. Duarte S, Baber J, Fujii T, Coito AJ. Matrix metalloproteinases in liver injury, repair and fibrosis. *Matrix Biol*. 2015;44:147–156. doi:10.1016/j.matbio.2015.01.004
13. Hemmann S, Graf J, Roderfeld M, Roeb E. Expression of MMPs and TIMPs in liver fibrosis–a systematic review with special emphasis on anti-fibrotic strategies. *J Hepatol*. 2007;46(5):955–975. doi:10.1016/j.jhep.2007.02.003
14. Kurzepa J, Mdro A, Czechowska G, et al.. Role of MMP-2 and MMP-9 and their natural inhibitors in liver fibrosis, chronic pancreatitis and non-specific inflammatory bowel diseases. *Hepatobiliary Pancreat Dis Int*. 2014;13(6):570–579. doi:10.1016/S1499-3872(14)60261-7
15. Lee Y, Friedman SL. Fibrosis in the liver: acute protection and chronic disease. *Prog mol Biol Transl Sci*. 2010;97:151–200. doi:10.1016/B978-0-12-385233-5.00006-4
16. Wen Y, Lambrecht J, Ju C, Tacke F. Hepatic macrophages in liver homeostasis and diseases-diversity, plasticity and therapeutic opportunities. *Cell. Mol. Immunol*. 2021;18(1):45–56. doi:10.1038/s41423-020-00558-8
17. Dhar D, Baglieri J, Kisseleva T, Brenner DA. Mechanisms of liver fibrosis and its role in liver cancer. *Exp Biol Med*. 2020;245(2):96–108. doi:10.1177/1535370219898141
18. Martín-Sanz P, Casado M, Boscá L. Cyclooxygenase 2 in liver dysfunction and carcinogenesis: facts and perspectives. *World J Gastroenterol*. 2017;23(20):3572. doi:10.3748/wjg.v23.i20.3572
19. Yang H, Xuefeng Y, Shandong W, Jianhua X. COX-2 in liver fibrosis. *Clin. Chim. Acta*. 2020;506:196–203. doi:10.1016/j.cca.2020.03.024
20. Rumzhum N, Ammit A. Cyclooxygenase 2: its regulation, role and impact in airway inflammation. *Clin Exp Allergy*. 2016;46(3):397–410. doi:10.1111/cea.12697
21. Motiño O, Agra N, Brea Contreras R, et al.. Cyclooxygenase-2 expression in hepatocytes attenuates non-alcoholic steatohepatitis and liver fibrosis in mice. *BBA*. 2016;1862(9):1710–1723. doi:10.1016/j.bbadis.2016.06.009
22. Jeong SW, Jang JY, Lee SH, et al.. Increased expression of cyclooxygenase-2 is associated with the progression to cirrhosis. *Korean J Int Med*. 2010;25(4):364. doi:10.3904/kjim.2010.25.4.364
23. Gao JH, Wen SL, Yang WJ, et al.. Celecoxib ameliorates portal hypertension of the cirrhotic rats through the dual inhibitory effects on the intrahepatic fibrosis and angiogenesis. *PLoS One*. 2013;8(7):e69309. doi:10.1371/journal.pone.0069309
24. Paik Y-H, Kim JK, Lee JI, et al.. Celecoxib induces hepatic stellate cell apoptosis through inhibition of Akt activation and suppresses hepatic fibrosis in rats. *Gut*. 2009;58(11):1517–1527. doi:10.1136/gut.2008.157420
25. Chávez E, Segovia J, Shibayama M, et al.. Antifibrotic and fibrolytic properties of celecoxib in liver damage induced by carbon tetrachloride in the rat. *Liver Int*. 2010;30(7):969–978. doi:10.1111/j.1478-3231.2010.02256.x
26. Su W, Tai Y, Tang S-H, et al.. Celecoxib attenuates hepatocyte apoptosis by inhibiting endoplasmic reticulum stress in thioacetamide-induced cirrhotic rats. *World J Gastroenterol*. 2020;26(28):4094. doi:10.3748/wjg.v26.i28.4094
27. Tai Y, Zhao C, Zhang L, et al.. Celecoxib reduces hepatic vascular resistance in portal hypertension by amelioration of endothelial oxidative stress. *J Cell Mol Med*. 2021;25(22):10389–10402. doi:10.1111/jcmm.16968
28. Bitto N, Liguori E, Mura VL. Coagulation, microenvironment and liver fibrosis. *Cells*. 2018;7(8):85. doi:10.3390/cells7080085
29. Ramadan M, Aly AA, El-Haleem LEA, Alshammari MB, Bräse S. Substituted pyrazoles and their heteroannulated analogs—recent syntheses and biological activities. *Molecules*. 2021;26(16):4995. doi:10.3390/molecules26164995
30. Abbas AA, Abdellattif MH, Dawood KM. Inhibitory activities of bipyrazoles: a patent review. *Expert Opin Ther Pat*. 2022;32(1):63–87. doi:10.1080/13543776.2021.1953474
31. El-Gamal MI, Zaraei S-O, Madkour MM, Anbar HS. Evaluation of substituted pyrazole-based kinase inhibitors in one decade (2011–2020): current status and future prospects. *Molecules*. 2022;27(1):330. doi:10.3390/molecules27010330
32. Ríos M-C, Portilla J. Recent advances in synthesis and properties of pyrazoles. *Chemistry*. 2022;4(3):940–968. doi:10.3390/chemistry4030065
33. Mohamed LW, Shaaban MA, Zaher AF, Alhamaky SM, Elsahar AM. Synthesis of new pyrazoles and pyrozolo [3, 4-b] pyridines as anti-inflammatory agents by inhibition of COX-2 enzyme. *Bioorg Chem*. 2019;83:47–54. doi:10.1016/j.bioorg.2018.10.014
34. Mantzanidou M, Pontiki E, Hadjipavlou-Litina D. Pyrazoles and pyrazolines as anti-inflammatory agents. *Molecules*. 2021;26(11):3439. doi:10.3390/molecules26113439
35. Priya D, Gopinath P, Dhivya LS, et al.. Structural insights into pyrazoles as agents against anti-inflammatory and related disorders. *ChemistrySelect*. 2022;7(5):e202104429. doi:10.1002/slct.202104429
36. Faidallah HM, Rostom SA, Khan KA. Synthesis and biological evaluation of pyrazole chalcones and derived bipyrazoles as anti-inflammatory and antioxidant agents. *Arch Pharmacal Res*. 2015;38(2):203–215. doi:10.1007/s12272-014-0392-7
37. Faidallah HM, Rostom SA. Synthesis, anti-inflammatory activity, and COX-1/2 inhibition profile of some novel non-acidic polysubstituted pyrazoles and pyrano [2, 3-c] pyrazoles. *Arch Pharm*. 2017;350(5):1700025. doi:10.1002/ardp.201700025
38. Domiati S, Mehanna M, Ragab H, Nakkash Chmaisse H, El Mallah A. Investigation of chronic efficacy and safety profile of two potential anti-inflammatory bipyrazole-based compounds in experimental animals. *J Inflamm Res*. 2018;Volume 11:143–153. doi:10.2147/JIR.S157955
39. Domiati S, Mehanna M, Ragab H, Abd El Galil K, Nakkash-Chmaisse H, El Mallah A. Elucidation of the molecular mechanism underlying the anti-inflammatory activity of an effective and safe bipyrazole-based compound. *Inflammation Res*. 2019;68(5):379–386. doi:10.1007/s00011-019-01225-z
40. Arora M, Choudhary S, Singh PK, Sapra B, Silakari O. Structural investigation on the selective COX-2 inhibitors mediated cardiotoxicity: a review. *Life Sci*. 2020;251:117631. doi:10.1016/j.lfs.2020.117631
41. Khan S, Andrews KL, Chin-Dusting JPF. Cyclo-oxygenase (COX) inhibitors and cardiovascular risk: are non-steroidal anti-inflammatory drugs really anti-inflammatory? *Int J mol Sci*. 2019;20(17):4262. doi:10.3390/ijms20174262
42. Domiati SA, El Galil KH A, Abourehab MAS, Ibrahim TM, Ragab HM. Structure-guided approach on the role of substitution on amide-linked bipyrazoles and its effect on their anti-inflammatory activity. *J Enzyme Inhib Med Chem*. 2022;37(1):2179–2190. doi:10.1080/14756366.2022.2109025
43. Chahal S, Rani P, Kiran Sindhu J, et al.. Design and development of COX-II inhibitors: current scenario and future perspective. *ACS omega*. 2023;8(20):17446–17498. doi:10.1021/acsomega.3c00692
44. Ramajayam R. Medicinal chemistry of vicinal diaryl scaffold: a mini review. *Eur J Med Chem*. 2019;162:1–17. doi:10.1016/j.ejmech.2018.10.054
45. Unver E, Tosun M, Olmez H, Kuzucu M, Cimen FK, Suleyman Z. The effect of taxifolin on cisplatin-induced pulmonary damage in rats: a biochemical and histopathological evaluation. *Mediators Inflamm*. 2019;2019:1–6. doi:10.1155/2019/3740867

46. Helppi J. Introducing International Council For Laboratory Animal Science (ICLAS). *Physiol Res*. 2023;72(5):P8–P8.
47. Wang R, Wang J, Song F, Li S, Yuan Y. Tanshinol ameliorates CCl4-induced liver fibrosis in rats through the regulation of Nrf2/HO-1 and NF-κB/IκBα signaling pathway. *Drug Des Devel Ther*. 2018;12:1281. doi:10.2147/DDDT.S159546
48. Ogaly HA, Eltablawy NA, El-Behairy AM, El-Hindi H, Abd-Elsalam RM. Hepatocyte growth factor mediates the antifibrogenic action of *Ocimum bacilicum* essential oil against CCl4-induced liver fibrosis in rats. *Molecules*. 2015;20(8):13518–13535. doi:10.3390/molecules200813518
49. Beutler E, Duron O, Kelly BM. Improved method for the determination of blood glutathione. *J Lab Clin Med*. 1963;61:882–888.
50. Ohkawa H, Ohishi N, Yagi K. Assay for lipid peroxides in animal tissues by thiobarbituric acid reaction. *Anal Biochem*. 1979;95(2):351–358. doi:10.1016/0003-2697(79)90738-3
51. Lee PY, Costumbrado J, Hsu C-Y, Kim YH. Agarose gel electrophoresis for the separation of DNA fragments. *JoVE*. 2012(62):e3923.
52. Abdellatif KR, Abdelall EK, Lamie PF, Labib MB, El-Nahaas E-S, Abdelhakeem MM. New pyrazole derivatives possessing amino/methanesulphonyl pharmacophore with good gastric safety profile: design, synthesis, cyclooxygenase inhibition, anti-inflammatory activity and histopathological studies. *Bioorg Chem*. 2020;95:103540. doi:10.1016/j.bioorg.2019.103540
53. Hevener KE, Zhao W, Ball DM, et al.. Validation of molecular docking programs for virtual screening against dihydropteroate synthase. *J Chem Inf Model*. 2009;49(2):444–460. doi:10.1021/ci800293n
54. Hasan KMM, Tamanna N, MAJFs H. Biochemical and histopathological profiling of Wistar rat treated with Brassica napus as a supplementary feed. *Food Sci Hum Wellness*. 2018;7(1):77–82. doi:10.1016/j.fshw.2017.12.002
55. Kulcsar-Gergely J, Kulcsar A. Studies on the effect of ursodesoxycholic acid on rats with acute carbontetrachloride injury. *Arzneimittelforschung*. 1997;47(5):659–661.
56. Singh P, Kaur S, Sharma A, Kaur G, Bhatti R. TNF-α and IL-6 inhibitors: conjugates of N-substituted indole and aminophenylmorpholin-3-one as anti-inflammatory agents. *Eur J Med Chem*. 2017;140:92–103. doi:10.1016/j.ejmech.2017.09.003
57. Gellibert F, Woolven J, Fouchet M-H, et al.. Identification of 1, 5-naphthyridine derivatives as a novel series of potent and selective TGF-β type I receptor inhibitors. *J Med Chem*. 2004;47(18):4494–4506. doi:10.1021/jm0400247
58. Van De Waterbeemd H, Gifford E. ADMET in silico modelling: towards prediction paradise?. *Nat rev Drug dis*. 2003;2(3):192–204. doi:10.1038/nrd1032
59. Lipinski CA, Lombardo F, Dominy BW, Feeney PJ. Experimental and computational approaches to estimate solubility and permeability in drug discovery and development settings. *Adv Drug Delivery Rev*. 2012;64:4–17. doi:10.1016/j.addr.2012.09.019
60. Veber DF, Johnson SR, Cheng H-Y, Smith BR, Ward KW, Kopple KD. Molecular properties that influence the oral bioavailability of drug candidates. *J Med Chem*. 2002;45(12):2615–2623. doi:10.1021/jm020017n
61. Ali MR, Kumar S, Afzal O, Shalmali N, Sharma M, Bawa S. Development of 2 (substituted benzylamino) 4 methyl 1, 3 thiazole-5-carboxylic acid derivatives as xanthine oxidase inhibitors and free radical scavengers. *Chem Biol Drug Des*. 2016;87(4):508–516. doi:10.1111/cbdd.12686
62. Elzahhar PA, Abd El Wahab SM, Elagawany M, et al.. Expanding the anticancer potential of 1, 2, 3-triazoles via simultaneously targeting Cyclooxygenase-2, 15-lipoxygenase and tumor-associated carbonic anhydrases. *Eur J Med Chem*. 2020;200:112439. doi:10.1016/j.ejmech.2020.112439
63. Hassan NW, Saudi MN, Abdel-Ghany YS, et al.. Novel pyrazine based anti-tubercular agents: design, synthesis, biological evaluation and in silico studies. *Bioorg Chem*. 2020;96:103610. doi:10.1016/j.bioorg.2020.103610
64. Nallagangula KS, Nagaraj SK, Venkataswamy L, Chandrappa M. Liver fibrosis: a compilation on the biomarkers status and their significance during disease progression. *Future Science OA*. 2017;4(1):FSO250. doi:10.4155/fsoa-2017-0083
65. Nicolas C, Wang Y, Nyberg SL. Cell therapy in chronic liver disease. *Curr Opin Gastroenterol*. 2016;32(3):189. doi:10.1097/MOG.0000000000000262
66. Burt AD, Ferrell LD, Hubscher SG. *MacSween's Pathology of the Liver E-Book*. Elsevier Health Sciences; 2017.
67. Majo J, Klinkhammer BM, Boor P, Tiniakos D. Pathology and natural history of organ fibrosis. *Curr Opin Pharmacol*. 2019;49:82–89. doi:10.1016/j.coph.2019.09.009
68. Koyama Y, Brenner DA. Liver inflammation and fibrosis. *J Clin Invest*. 2017;127(1):55–64. doi:10.1172/JCI88881
69. Tacke F. Targeting hepatic macrophages to treat liver diseases. *J Hepatol*. 2017;66(6):1300–1312. doi:10.1016/j.jhep.2017.02.026
70. Ramachandran P, Iredale JP, Fallowfield JA. Resolution of liver fibrosis: basic mechanisms and clinical relevance. *Semin Liver Dis*. 2015;35(2):119–131. doi:10.1055/s-0035-1550057
71. Tacke F, Trautwein C. Mechanisms of liver fibrosis resolution. *J Hepatol*. 2015;63(4):1038–1039. doi:10.1016/j.jhep.2015.03.039
72. Liedtke C, Luedde T, Sauerbruch T, et al.. Experimental liver fibrosis research: update on animal models, legal issues and translational aspects. *FibrogenTissue Repair*. 2013;6:1–25. doi:10.1186/1755-1536-6-19
73. Heyens LJM, Busschots D, Koek GH, Robaeys G, Francque S. Liver fibrosis in non-alcoholic fatty liver disease: from liver biopsy to non-invasive biomarkers in diagnosis and treatment. *Front Med*. 2021;8:615978. doi:10.3389/fmed.2021.615978
74. Hui AY, Leung WK, Yuen Chan HL, et al.. Effect of celecoxib on experimental liver fibrosis in rat. *Liver Int*. 2006;26(1):125–136. doi:10.1111/j.1478-3231.2005.01202.x
75. Wang Y, Wang S, Wang R, Li S, Yuan Y. Neferine exerts antioxidant and anti-inflammatory effects on carbon tetrachloride-induced liver fibrosis by inhibiting the MAPK and NF-κB/IκBα pathways. *Evid Based Complement Alternat Med*. 2021;2021:4136019
76. Comporti M, Saccocci C, Dianzani MU. Effect of CCl-4 in vitro and in vivo on lipid peroxidation of rat liver homogenates and subcellular fractions. *Enzymologia*. 1965;29(3):185–204.
77. Ghoshal AK, Recknagel RO. Positive evidence of acceleration of lipoperoxidation in rat liver by carbon tetrachloride: in vitro experiments. *Life Sci*. 1965;4(15):1521–1530. doi:10.1016/0024-3205(65)90173-6
78. Dat NQ, Thuy LTT, Hieu VN, et al.. Hexa histidine–tagged recombinant human cytoglobin deactivates hepatic stellate cells and inhibits liver fibrosis by scavenging reactive oxygen species. *Hepatology*. 2021;73(6):2527–2545. doi:10.1002/hep.31752
79. Narayanankutty A, Job JT, Narayanankutty V. Glutathione, an antioxidant tripeptide: dual roles in carcinogenesis and chemoprevention. *Curr Protein Pept Sci*. 2019;20(9):907–917. doi:10.2174/1389203720666190206130003
80. Feldman M, Friedman LS, Brandt LJ. Sleisenger and Fordtran's gastrointestinal and liver disease: pathophysiology, diagnosis, management. *Elsevier Health Sci*.
81. Drisko JA. Chelation Therapy. In: Rakel D, editor. *Integrative Medicine*. 4th ed. Amsterdam: Elsevier; 2018:1004–1015.e1003.

82. Gaweł S, Wardas M, Niedworok E, Wardas P. Malondialdehyde (MDA) as a lipid peroxidation marker. *Wiad Lek*. 2004;57(9–10):453–455.
83. El-Haskoury R, Al-Waili N, Kamoun Z, Makni M, Al-Waili H, Lyoussi B. Antioxidant activity and protective effect of carob honey in CCl4-induced kidney and liver injury. *Arch Med Res*. 2018;49(5):306–313. doi:10.1016/j.arcmed.2018.09.011
84. Yang YM, Seki E. TNFα in liver fibrosis. *Curr Pathobiol Rep*. 2015;3(4):253–261. doi:10.1007/s40139-015-0093-z
85. Li H, Adamopoulos IE, Moulton VR, et al.. Systemic lupus erythematosus favors the generation of IL-17 producing double negative T cells. *Nat Commun*. 2020;11(1):2859. doi:10.1038/s41467-020-16636-4
86. Dang SS, Wang BF, Cheng YA, Song P, Liu ZG, Li Z. Inhibitory effects of saikosaponin-d on CCl4-induced hepatic fibrogenesis in rats. *World J Gastroenterol*. 2007;13(4):557. doi:10.3748/wjg.v13.i4.557
87. Abdelghany AH, BaSalamah MA, Idris S, Ahmad J, Refaat B. The fibrolytic potentials of vitamin D and thymoquinone remedial therapies: insights from liver fibrosis established by CCl4 in rats. *J Transl Med*. 2016;14:1–15. doi:10.1186/s12967-016-1040-4
88. Hafez MM, Hamed SS, El-Khadragy MF, et al.. Effect of ginseng extract on the TGF-β1 signaling pathway in CCl4-induced liver fibrosis in rats. *BMC Complement Altern Med*. 2017;17(1):1–11. doi:10.1186/s12906-016-1507-0
89. Ftahy MM, Latif NSA, Alalkamy EF, El-Batrawi FA, Galal AH, Khatab HM. Antifibrotic potential of a selective COX-2 inhibitor (celecoxib) on liver fibrosis in rats. *Comp Clin Pathol*. 2013;22(3):425–430. doi:10.1007/s00580-012-1427-4
90. Fahmy HT, Rostom SA, Saudi MN, Zjawiony JK, Robins DJ. Synthesis and in vitro evaluation of the anticancer activity of novel fluorinated thiazolo [4, 5-d] pyrimidines. *Arch Pharm*. 2003;336(4-5):216–225. doi:10.1002/ardp.200300734
91. Noriega S, Cardoso-Ortiz J, López-Luna A, Cuevas-Flores MDR, Flores De La Torre JA. The diverse biological activity of recently synthesized nitro compounds. *Pharmaceuticals*. 2022;15(6):717. doi:10.3390/ph15060717
92. Hernandes MZ, Cavalcanti SMT, Moreira DRM, de Azevedo Junior WF, Leite ACL. Halogen atoms in the modern medicinal chemistry: hints for the drug design. *Current Drug Targets*. 2010;11(3):303–314. doi:10.2174/138945010790711996